POLITEHNICA UNIVERSITY OF BUCHAREST

Doctoral School in Engineering and Applications of Lasers and Accelerators

Decision No. from

Summary of Ph.D. THESIS

Alexandru-Nicolae STATE

TRANSPORTUL ȘI EXTRACȚIA IONILOR FOLOSIND CURGERI DE GAZ ÎN SISTEME DE CAPTURĂ A IONILOR DE ULTIMĂ GENERAȚIE

ION TRANSPORT AND EXTRACTION WITH GAS FLOWS IN NEXT GENERATION ION CATCHERS

THESIS COMMITTEE

CS1 Dr. Ing. Călin A. Ur IFIN-HH/ELI-NP	President
Prof. Dr. Dimiter L. Balabanski IFIN-HH/ELI-NP	PhD Supervisor
CS2 Dr. Nikolay Djourelov IFIN-HH/ELI-NP	Referee
Prof. Dr. Christoph Scheidenberger University of Giessen/GSI	Referee
Assoc. Prof. Dr. Alexandru Nicolin University of Bucharest	Referee

BUCHAREST 2022

Acknowledgements

I would like to thank all the people that helped me during this endeavor. It has been an amazing journey. But all things must come to an end in order for others to start.

I would like to thank my scientific coordinator, Prof. Dr. Dimiter Balabanski, for the invaluable suggestions, support and help during the last five years. I would also like to thank Dr. Paul Constantin for all the help and careful consideration of all the work. Without your guidance this thesis would not have been possible. I would like to thank Dr. Horia Petrașcu for all the help and guidance when working on the 4th experimental line of the 9 MV accelerator of IFIN-HH. I would like to also thank Dr. Dan Ghiță for all the help and guidance throughout the last decade from which i have learned tremendously.

I would like to thank the entire FRS Ion Catcher group especially: Dr. Timo Dickel, Dr. Wolfgang Plass, Soenke Beck, Daler Amanbayev and all the other group members, for the opportunities of working at such an amazing experimental setup while gathering invaluable experience for the years to come. Moreover, i would like to thank Dr. Holger Brand for all the patience and help whilst learning CS++.

Last but not least, i would like to thank my parents Daniela and Adrian and my grandmother Maria for the life-time support and to my wife Dana and our son Tudor. I appreciate everything that was done. Thank you!

Table of contents

Chapter 1

Introduction

Our thirst for knowledge has led to the discovery of thousands of unstable or radioactive nuclides and many more will remain to be discovered by the passage of time. Exotic nuclei have been/are characterized for many years. They are exotic through their particularities: short half-lives and radioactive, two arguments that increase the overall complexity and difficulty when trying to study them. Nevertheless, these studies help test the extremes of current nuclear models and their validity. Before detailing why exotic nuclei are important, some basic concepts will be further introduced.

One important concept in nuclear physics is represented by the valley of stability. As the name implies, it is a form of characterizing the nuclides stability based on their binding energy. The latter can be written as:

$$B(N,Z) = NM_n + ZM_p - M(N,Z) \tag{1.1}$$

where $M(N,Z)$ is the mass, $M_{n,p}$ are the nucleon masses.

Of course, this valley has a specific profile. This is defined by the stable nuclei. The lowest part of this valley is where the most stable nuclei reside. If we were to draw a line through the center of the valley, we would get the line of β stability. Any combination of protons and neutrons does not result in a stable nucleus. By adding one nucleon at a time, moving up (adding protons) and/or right (adding neutrons) across the table of nuclides, at some point the newly formed nucleus will decay rapidly with the emission of a proton or a neutron. Informally speaking, the nucleon is said to have dripped out of the nucleus from which the term dripline appeared. These driplines define the valley limits of existence of bound nuclei.

In the context of exotic nuclei, although they do not occur naturally on Earth, they play an important role in the life and death of stars. Like stated before, stable nuclei account for a small part of all the possible configurations of nucleons in nuclei. Most of them have been studied and their global properties are well known (mass, parity, radius etc.) as well as their method of creation. Light elements like Hydrogen, Helium, Lithium, Beryllium and Boron are known to be produced right after the Big Bang, and up to iron

they are created in the hot interiors of stars, with very well-defined stages of nuclear burning. For a lot of nuclides there is still much work to be done, especially at high excitation energies, in order to define their complex structure like excited states, spins, parities etc.

The above-mentioned study represents the complex puzzle of nuclear astrophysics. The purpose of this puzzle is to answer the how, where and when the elements in the universe were created and explain their abundance. Stars suffer a never-ending story of continuous evolving as the elemental constituents that form the star start to change by hydrogen burning (main sequence star), helium burning (red giant star) and so on (burning of higher elements). Depending on their mass, low-mass stars will slowly eject its atmosphere (stellar wind), thus forming a planetary nebula whilst a high-mass star will eject mass by undergoing a powerful and luminous explosion called a supernova. For elements above iron, the $r-$, $s-$ processes (rapid or slow neutron capture), $rp-$, $p-$ processes (rapid proton or proton capture) have been determined. As such, studies and measurements of these processes have important applications in nuclear astrophysics and the understanding of nuclear structure.

The research scope of physicists related to studies of exotic nuclei is thus complex, having to deal with very short half-lives and the challenges of producing them artificially with various techniques. Another problem that accelerator physicists have to deal with is making sure there is enough of these nuclei to create accelerated beams in order to study their interaction with other nuclei. Being unstable and having a short lifetime (more exotic means shorter lifetime) makes it difficult to capture these exotic nuclei, also considering the low production cross-sections. Analyzing them becomes difficult considering that most of the time common nuclei are produced at the same time, with orders of magnitude more.

The current and most important methods of producing and separating exotic nuclei are the Isotope soparation on-line (ISOL) which is followed by post-acceleration and the in-flight separation (IFS) methods which will be treated in more detail in the next chapter of this summary. The ISOL technique uses an intense primary beam of light-particles, usually produced with the help of a particle accelerator or a nuclear reactor, to hit a thick and hot target. This interaction will form many stable and unstable nuclei. As we are mainly interested in the unstable, exotic nature of the produced nuclei, after they are produced, they diffuse into an ion source where they are ionized and extracted. There are many RIB production facilities around the world that utilize the ISOL method like the ones at ISOLDE (CERN), ALTO (IPN Orsay), TRIUMF (Vancouver) etc. These facilities are used for mass and isobar selection with mass spectrometers, with primary beams that have good optical properties as they rely only on the ion source. The limits of the ISOL technique is reached when extraction and ionization is not sufficient to distinguish the nuclei of interest, due to the chemistry of the produced elements. An

example of such a limit is the study of refractory elements that have an evaporation temperature above 1500 K.

While the ISOL method is dependent of the chemistry of the produced elements, the in-flight method is independent but has as a drawback the optical quality which is not that great, leading to the requirement of mass separators with greater acceptance. This technique is based on the interaction of a heavy-ion beam with a thin target, leading to fragmentation that transfers their momentum to the reaction products which have comparable energies with the incident beam. Several fragmentation facilities exist around the world, namely NSCL (USA), ETNA fragment separator at LNS (Italy), COMBAS and ACCULINA separator at JINR (Russia), FRS fragment separator at GSI (Germany), RIBF at RIKEN (Japan), GANIL (France) etc.

In the 1980s, the Ion Guided Isotope Separation On-Line (IGISOL) method started to emerge in Jyvaskyla (Finland) by using a gas-filled stopping cell. The exotic nuclei after being produced via fission with a proton beam on an uranium target placed inside the gas cell, were slowed down, hence the term stopping, to kinetic energies of eV, thermalized and delivered to high precision low-energy experiments for mass spectrometry, decay spectroscopy or laser spectroscopy. Of high importance when using gas cells are the density which affects the stopping power and cleanliness. The latter will impact the charge state of the products and in order to avoid neutralization, an ultra pure gas is preferred.

Fast forwarding till present time, 2022, at GSI (Germany) the Ion Catcher setup uses a cryogenic stopping cell (CSC) to slow down and thermalize fragments produced by the FRS fragment separator. These fragments are produced either by projectile fragmentation or fission at relativistic energies, separated using an in-flight method and slowed down in the CSC. A multiple reflection time-of-flight spectrometer is used for mass measurements and to provide an isobarically clean beam for further experiments, like mass or decay spectroscopy. Different aspects of this setup will be discussed within several chapters of the thesis. Moreover, this setup and this generation of a longitudinal, cryogenic stopping cell has been an early prototype for the future CSC with an orthogonal extraction that will be built and used on the Low Energy Branch of the future SuperFRS. As this is an extremely anticipated and unique project, starting from the design firstly introduced in [1], many research institutes around the world (ELI-NP - Romania, GSI and Giessen University - Germany, Soreq and Tel Aviv University - Israel, JYFL - Finland) have decided to support the HADO-CSC (High Area Density Orthogonal Extraction Cryogenic Stopping Cell) project.

There has been tremendous scientific progress and interest whilst trying to explain the unknown, as all the above-mentioned facilities try to cover new parts of the nuclide chart. Research and development in the nuclear field has always led to technological advancements in various other fields. Following this idea, the Extreme Light Infrastructure – Nuclear Physics (ELI-NP) is one of the research infrastructures in the world

focused on photonuclear physics. The project comprises of two important equipment: the high-power laser system with two 10 PW ultra-short pulse lasers and a highly brilliant gamma-ray beam system, with energies up to 19.5 MeV. The latter will provide a new research instrument of great importance in which gamma beam energies will cover the GDR (Giant Dipole Resonance) of Uranium and Thorium isotopes making it ideal for photo-fission experiments.

As one of the two important equipment at ELI-NP, the high-brilliance gamma beam is more than capable for the production and studies of fission fragments. Thus, based on the experience with the Ion Catcher prototype CSC, an experimental program has risen at ELI-NP in the form of the ELISOL project in which one of the most important topics is the development of a new CSC with a different geometry. This is a two-chamber gas cell with an orthogonal extraction which should provide an extraction time in the tens of milliseconds, which will be used to slow down and thermalize the fission products that are formed after the interaction of the gamma beam with the actinide targets placed inside the first chamber, called the stopping chamber.

Moreover, this experimental program aims at producing exotic neutron-rich radioactive ion beams, or RIBs, in order to investigate refractory elements in the Zr-Rh region with masses A$\approx$100 and the rare earth region with masses around 140. To accomplish this, the IGISOL technique is used. The estimated $5 \cdot 10^{10}\gamma$/s flux of the primary beam with energies between 10.2 – 19.5 MeV [2] will hit thin actinide targets leading to a photo-fission reaction in which the fission products will be collected and delivered as an ion beam. This is realized by using DC, RF fields and supersonic jets.

The thesis is structured in six sections. The first two chapters cover a brief introduction of the thesis and describe the current research with exotic nuclei around the world. At the same time, chapter two emphasizes the conceptual design of the cryogenic stopping cell to be used at ELI-NP. Chapter three and four cover the modeling principles for computational fluid dynamics with an emphasis on Laval nozzles and how supersonic jets are formed and used in the new stopping cell. Also the design of the helium recovery unit will be presented, a recirculation gas system for the HADO-CSC. Chapter five covers the mechanical design, construction, simulation and testing of a test unit to be used for applying different invasive and non-invasive techniques for characterizing supersonic jets with the results applicable to the HADO-CSC. Chapter six covers slow control systems used for nuclear physics in LabVIEW. The emphasis will be placed on two distinct control systems, implemented in LabVIEW but with a different design pattern. The queued message handler (QMH) was used to automate the scattering chamber on the 4^{th} experimental line of the 9 MV Tandem accelerator of IFIN-HH. The Actor Framework with CS++ was used for the slow control development of the FRS Ion Catcher setup at GSI (Germany).

Chapter 2

Radioactive ion beams. Overview of production methods.

The focus is on the IGISOL method and how it is applied at ELI-NP within the Radioactive Ion beam (RIB) facility. As such, this chapter covers the formation and separation of exotic nuclei and how they are used as a RIB for further studies. Furthermore, the basics of the used methodologies in state-of-the-art facilities around the world where RIBs are produced and used in different experimental setups are briefly described in the current summary.

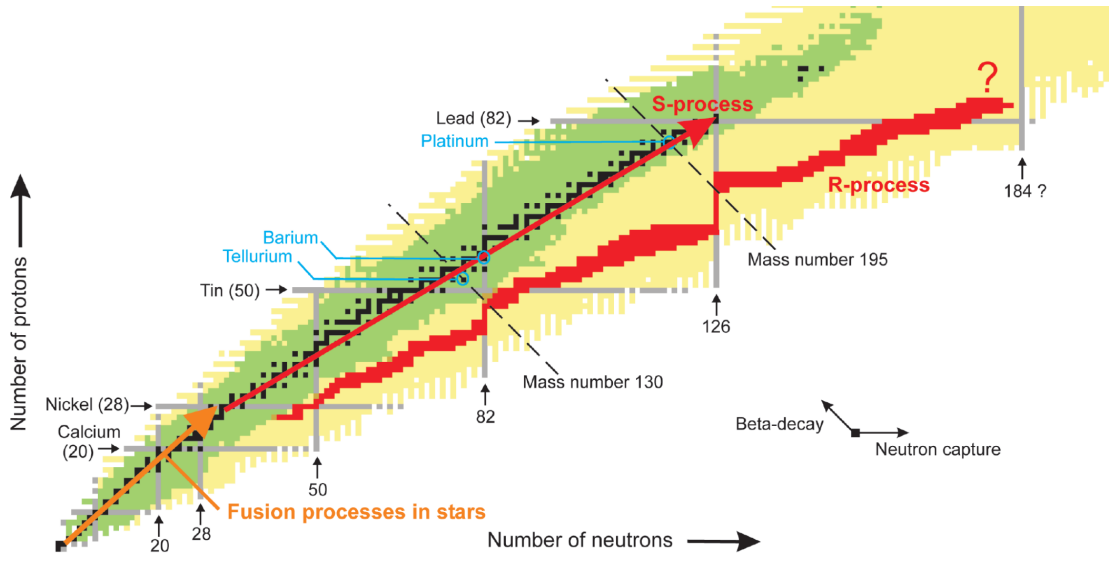

Fig. 2.1 Nuclide chart displaying the stable nuclei with solid black, the region of discovered nuclei is in the green region with an approximation of the unknown and undiscovered ones in the yellow region. The red arrow close to the stable nuclei is the s-process (slow neutron capture). The r-process (rapid neutron process) is represented by the red band going through the undiscovered neutron-rich nuclei region in yellow. [3]

Fig. 2.1 displays the chart of nuclides, a two-dimensional representation of all known isotopes. One axis represents the neutron number (N) while the other represents

the proton number (Z). Each point on this chart, characterized by (N,Z) coordinates represents a specific nuclide of a chemical element. The solid black symbols indicate stable nuclei. This belt of stability, where stable nuclei reside, makes it easy to distinguish between the different areas where alpha decay, β^+ (positron emission), β^- (electron emission) occur. Unstable nuclei tend to follow a decay pathway, subsequently occurring until reaching a stable nucleus on the belt.

For a complete picture and understanding of the nuclide chart and the r-, s- processes (neutron capture), depicted in Fig. 2.1 some fundamental ideas have to be introduced. Chemical elements are created within stars by combining protons and neutrons from lighter elements. This process is called nucleosynthesis. There are three main types: Big Bang, Stellar and Supernova nucleosynthesis. All three are related to the formation and evolution of the Universe as we know it. These phases have been briefly described in the thesis.

2.1 Methods of RIB production and separation

As one moves from the valley of beta-stability, producing exotic nuclei becomes more and more difficult to accomplish. Studies of isotopes with very different proton to neutron ratios, when compared to stable isotopes, are quite troublesome. The challenges that different methods of production must overcome are the short half lives of the nuclei of interest, the low production cross sections and the fact that during a nuclear reaction multiple other species are produced.

Two complementary methods have been developed and refined in the last decades to produce radioactive ion beams, i.e., the isotope separation on-line (ISOL) and the in-flight techniques. Both of them try to fulfill different requirements for specific experiments that cover different parts of the nuclide chart. There is no method to cover everything and each comes with its advantages and disadvantages. The most important properties when discussing methods of producing exotic nuclei are [4]:

- **Good production rate.** This requires a very good optimization of the primary beam in terms of intensity.
- **Efficiency.** The system of production has to be as close as possible to unity.
- **Selectivity.** The isotopes of interest, in this case unstable and short-lived, have to be separated, out of all the resulting nuclear reaction products, effectively.
- **Fast.** Short-lived exotic nuclei decay very fast. As such, the time between production and arrival at the detector set-up has to be kept to a minimum.

Figure 2.2 displays the schematic representations of the two methods of producing RIBs. The in-flight method, depicted on top, and the ISOL method, on bottom.

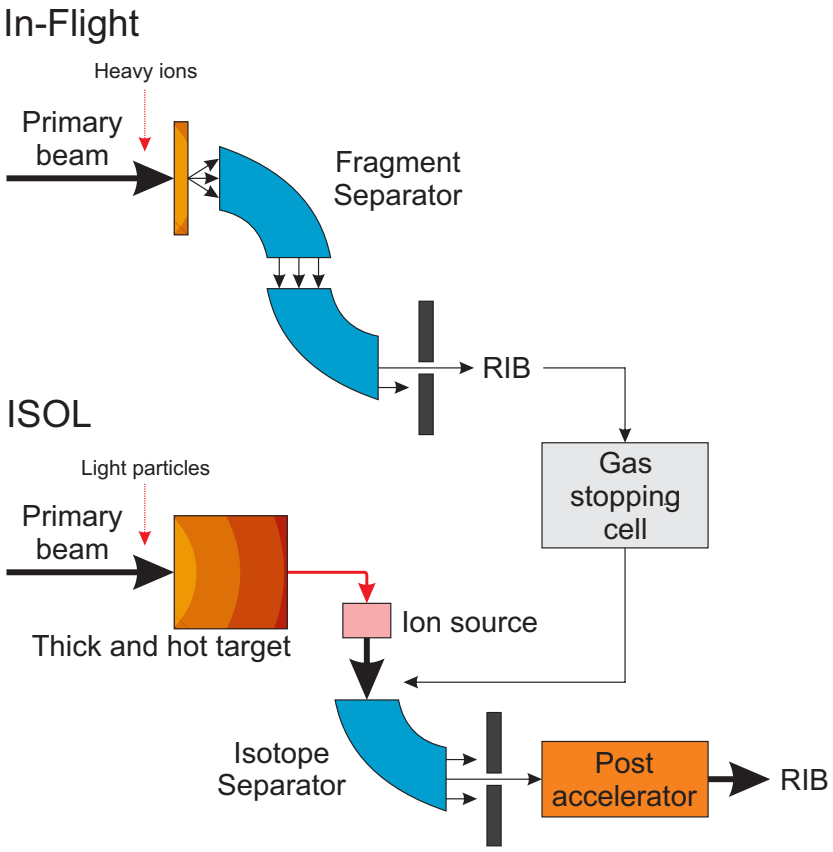

Fig. 2.2 Schematic drawings of the In-flight and ISOL techniques. Moreover, the in-flight method using an ion catcher is also presented.

2.1.1 ISOL and IGISOL

The Isotope Separation On-Line (ISOL) method is used at several facilities in the world to produce exotic nuclei. The latter are produced by nuclear interactions of light particles colliding on targets made out of materials with a high atomic number (Z).

A thick target is usually used to stop the reaction products. Once stopped they are neutralized in the target and later on will diffuse due to the high temperatures to which the target is heated. In contrast to the IGISOL (Ion-Guided Isotope Separation On-Line) technique in which the reaction products of interest "survive" neutralization, and DC fields can be used to guide them, in the ISOL method an ion source is needed. This makes sure to ionize, accelerate and further separate the products of interest [5].

Furthermore, the thick targets (2-10 cm) used in the ISOL technique will provide high production rates, but slow release by thermal diffusion. The heating at $\approx$ 2000°C makes the production cell an oven in which electrical extraction is not possible, which results in a slow extraction time from the cell. The IGISOL technique, in which the thin targets are used (2-10 μm) leads to small production rates but a fast release by kinematical recoil. The cell in which the targets are placed can be filled with gas for stopping and DC fields can be used for extraction. This leads to an overall fast extraction time.

Moreover, as high temperatures, in the range of thousands of °C, are needed to make the atoms of interest diffuse out of the bulk of the target towards the surface, and towards the ion source, some elements are very difficult to produce. For example, refractory elements that have a high evaporation temperature. This is the advantage of the gamma beam system coupled with the cryogenic stopping cell at ELI-NP that permits the production of exotic neutron rich fission fragments with two main important regions: the refractory elements in the light region of Zr-Mo-Rh and the Heavy rare-earths region around Ce.

2.1.2 In-flight method

The in-flight method was firstly developed at Lawrence Berkeley Laboratory (LBNL) in the 1970s at the Bevalac accelerator [6] and later on improved at the LISE separator at GANIL by the adoption and use of degraders. The in-flight method complements the ISOL technique which, as stated before, covers different regions of the nuclide chart. This is possible by the use of a heavy-ion beam which generally hits a thin target. This forward momentum of the incident fragments is used for separating by mass or further inducing other reactions. The reaction products, of high kinetic energy, are able to go through the thin target, continue towards the ion optics elements and afterwards separated by magnetic or electric fields.

As stated before, each method comes with its own pros and cons which is an experimental physicist's primary dilemma many times in the early stages of an experiment. The in-flight method is chemistry independent but due to the primary fragments interaction with the thin targets, mass separators with high acceptance have to be designed and used. Moreover, the in-flight intensity is generally lower than that of the ISOL primary beam, resulting in a lower yield for some exotic fragments [7].

2.1.3 In-flight systems paired with stopping cells

In the in-flight technique one has to take into account that the nuclei of interest will have high velocity, thus high kinetic energy and spatially will cover a large phase space.

In terms of ion manipulation for spectroscopy of exotic nuclei there are certain measurements that are in use, i.e., mass measurements, decay spectroscopy, collinear laser spectroscopy and ToF mass measurements. These are all applicable to secondary beams of tens of eV. As such, the primary beam, of high kinetic energy, has to be shaped in such a way that its emmitance is small, can be bunched, and its energy is reduced, so the nuclei are stopped in a controlled gaseous environment. The latter represents a gas catcher.

A schematic representation of a gas catcher, based on the working principle of the one that can be found at the FRS Ion Catcher, at GSI, is represented in Fig. 2.3.

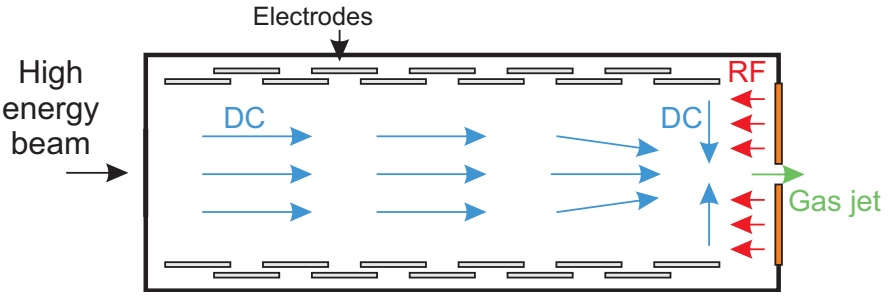

Fig. 2.3 Schematic drawing of the forces involved in a gas catcher. The electrodes that form a DC cage provide a DC push field that drift the charged particles towards an RF type structure. In this particular case an RF carpet was considered which provides a radial DC field to push the ions towards the center and a RF component which repels the ions from hitting the surface. In the middle of the RF carpet a cylindrical nozzle exists and due to the pressure difference, a gas jet will be used as a guiding mechanism to push the ions towards a mass separator.

Although the gas catcher represented in Fig. 2.3 requires the use of an RF Carpet, as in the case of the FRS Ion Catcher setup, a generality can be found in the use of a high-density neutral gas, a longitudinal DC push field, and an RF type structure to push the ions out of the gas catcher. Each facility will provide different methodologies or geometries also based on their particular interests and possibilities given the primary beam and way of production. For example, the CARIBU gas catcher meant for delivering neutron-rich fission fragments at low and Coulomb barrier energies, presents a conical shape RF structure meant to stop the radial expansion of the ions during transport due to diffusion in the gas and the space charge in the volume [8].

Furthermore, as a monoenergetic radioactive beam enters the gas cell, the exotic nuclei will lose energy by the interaction with the buffer gas and thermalize. The thermalization process is one of the key features that permitted the development of the IGISOL technique as the "stopped" exotic nuclei remain in a charged state so a DC electric field can be used to push them towards the exit and towards the mass separator. Furthermore, helium gas is usually used in gas cells for the process of thermalization, due to its high ionization potential. Otherwise, if meant to neutralize the exotic nuclei, a gas like argon can be used.

After thermalization, the particles of interest are transported towards the exit nozzle where a Radio Frequency (RF) carpet (multiple concentric electrodes presenting a sub-mm nozzle in the middle) will push the particles towards the center and the RF fields will prevent the ions from being neutralized by hitting the walls. When reaching the nozzle area, the drag force exerted by the gas jet will be strong enough to guide the ions towards the rest of the beamline. Typically, after the gas cell, a low pressure region is met. This region is accompanied by RFQs (Radio Frequency quadrupoles) or different optical elements meant for confining the extracted ions.

2.2 Possibilities for RIB production in photo-nuclear reactions

ISOL facilities around the world use different materials as targets: from metallic foils to liquids to poly-phasic mixed uranium carbides [9]. What they have in common is the use of a thick target, heated to temperatures of around 2000°C. This process permits the diffusion out of the target of the fission fragments which later on get re-ionized. The primary beam that leads to the fission products of interest can be, e.g., either highly energetic protons like in the case of ISOLDE (CERN) [10], or a bremmstrahlung γ beam like in the case of the ALTO facility [11].

The ISOL method although it provides significant advantages and provides a significant particle current it is not a perfectly suited technique to cover and produce any unstable beam. More specifically, refractory elements are very difficult or impossible to produce as they have high evaporation temperatures, in some cases above 3500°C and the overall process of evaporation and diffusion is slow, in the hundreds of ms. The quest for the discovery of newer short lived isotopes also implies new ways of RIB formation and its underlying reaction, minimizing the extraction time.

The forthcoming developments regarding the ELI-NP project will bring it closer to the operational stage in which a tunable gamma-ray beam, produced via compton backscattering, with energies up to 19.5 MeV, will be used. This energy is sufficient to cover the giant dipole resonance (GDR) of ^{238}U and ^{232}Th.

Similarly to the gas cell depicted in 2.3, in which the highly energetic fragments are stopped in a gas cell and shaped in the form of a RIB, a gamma beam can be used as the primary beam, which will create the fission products of interest via the process of photo-fission. Placing numerous thin targets axially along the gamma beam, results in production of fission products which are released with a high kinetic energy, and then stopped in a controlled density, that of the used gas cell.

Although the problem of producing refractory elements (which can be released by kinematical recoil and not by thermal diffusion) is resolved by the use of the IGISOL method based on thin targets, the possibilities of forming RIBs out of shorter-lived isotopes, compared to the current technical limits have to be investigated.

The design presented in 2.3 presents the working principle of the current FRS Ion Catcher CSC. This gas cell provides an extraction time of $\approx$ 25 ms (Off-line measurement with ^{219}Rn ions [12]). The HADO-CSC design is expected to extract below $\approx$10 ms with twice the length of the CSC (which would lead to a 50 ms extraction time). A factor larger than five is resulted, which will have a great impact, having in mind the exponential dependence on time.

2.2.1 HADO-CSC working principle

The HADO-CSC is one of the proposed experimental setups that will make use of the gamma beam system. This is a two-chamber gas cell with an orthogonal extraction, meant to provide short extraction times in the range of milliseconds [13]. Such a design has been firstly proposed to be used with the Super-FRS at GSI [1], being an upgrade of the existing one [14].

The conceptual design of the HADO-CSC is emphasized in Figure 2.4. In the helium gas, the fission products undergo a thermalization process in which a large fraction of the reaction products reach a 1+ charge state [15]. Strong DC fields ($\approx$100V/cm) drift the ions out in an orthogonal direction to the impinging gamma beam. This assures a quicker extraction path than a longitudinal geometry, thus it minimizes the extraction time. The use of DC electrical fields is highly important in the design stage of any gas cell, as it directly impacts the transport time of the produced heavy ions drifting in thermal motion.

Moreover, the DC field should be designed in such a way that it covers the entire volume of the gas cell. Many metallic electrodes, that commonly form a DC Cage, are connected to a voltage divider, to form a symmetric DC field. Several remarks have to be mentioned when using electrical fields with gas cells. Firstly, helium gas is preferred due to its high ionization potential that limits neutralization of the fission products via electron capture. The gas cell cleanliness is of great importance, as the impurities can lose electrons with ease and neutralize the heavy ions of interest. The cleanliness is meant to be better than 1 ppb. This is achieved by continuously recirculating the used gas through various active and passive getters. Moreover, the use of cryogenics is desired in order for the impurities to get frozen to the walls and permit a higher stopping power due to the increased density. The methodology of reaching such a high purity level will be stressed out in section 4.4 where a recirculation gas unit is presented. Secondly, before the process of thermalization, the highly energetic fission products are released from the thin targets with high kinetic energies. During this process, the neutral He atoms become ionized, leading to the formation of a low-temperature plasma. This space-charge effect accumulates over time and can eventually lead to the cancellation of the electric field. This effect is undesirable as the ion extraction is dependent on the electric field. What is extremely important with such a gas cell design is the fact that with the same voltages applied on the DC Cage electrodes the electric fields will be higher. This permits the operation of the HADO-CSC with a 5 orders of magnitude higher space charge than the current standard longitudinal extraction gas cells [1, 16].

Furthermore, close to the stopping chamber wall, multi-layered printed circuit boards (RF Carpets) are used as a guiding mechanism for the charged fission products which get in close proximity. Frequencies of up to 8 MHz are used to repel the ions from sticking to the wall. Eq. 2.1 [17, 18] gives the average repelling force of an RF carpet.

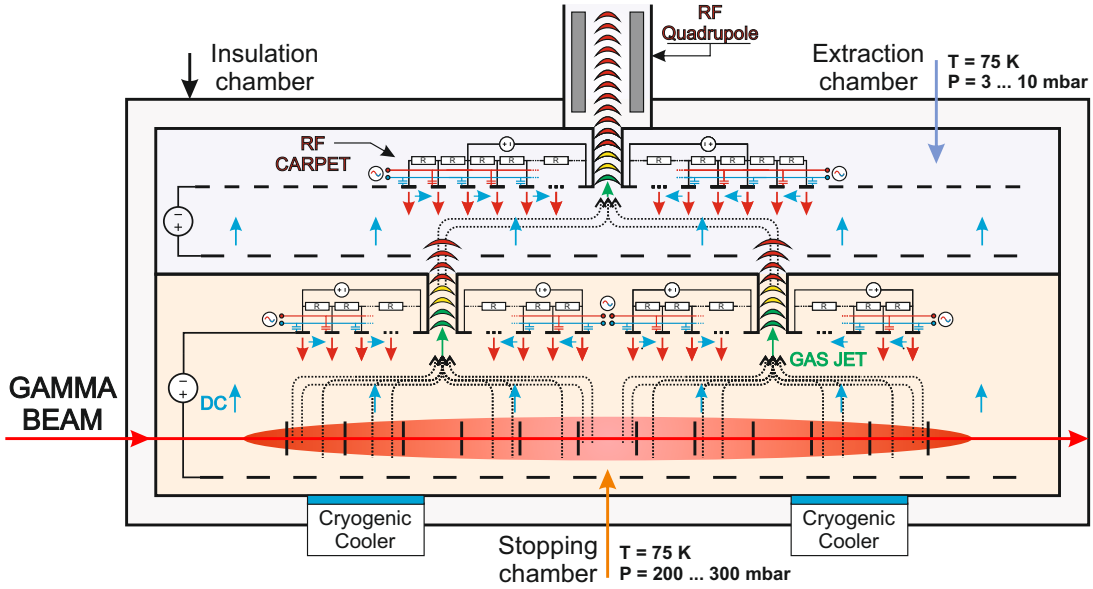

Fig. 2.4 Conceptual design of the HADO-CSC: photo-fission region in red, ion trajectories in black, DC fields in blue, RF fields in red, gas jets in green.

$$F_{avg} = m \cdot \left(\mu_0 \frac{\rho_0}{\rho}\right)^2 \cdot \frac{V_{RF}^2}{r_0^3} \tag{2.1}$$

where: m - ion mass, μ_0 - reduced ion mobility, ρ_0 - normal gas density, ρ - gas density, V_{RF} - RF Amplitude, r_0 - half electrode spacing.

Eq. 2.1 provides several design criteria to be taken into consideration. An increased density in the cell will lead to the need of an increased RF amplitude or a decrease in the electrode spacing. The latter has a stronger effect than when increasing the RF amplitude due to the higher power.

Furthermore, in the middle of the RF carpet a sub-mm cylindrical hole will act as a guiding mechanism for the fission products. These will be guided by the drag force generated by an almost hypersonic jet (Mach no. > 5) formed due to the difference in pressure between the two chambers of the stopping cell (200-300 mbar) in the lower stopping chamber and low pressure (3-10 mbar) in the upper extraction chamber. The emphasis in the following chapters will be on the gas jet dynamics in the HADO-CSC.

Chapter 3

Modeling principles for computational fluid dynamics

3.1 Computational fluid dynamics - modeling principles

This chapter presents the main considerations of computational fluid dynamics simulations. The latter use algorithms that rely on numerical approximations in order to find a solution to a fluid flow physical phenomenon. They take into consideration velocity, temperature, pressure, thermal effects, viscosity etc. Common uses of CFD simulations are found in aerodynamics and aerospace, biological and environment engineering, automotive industry etc.

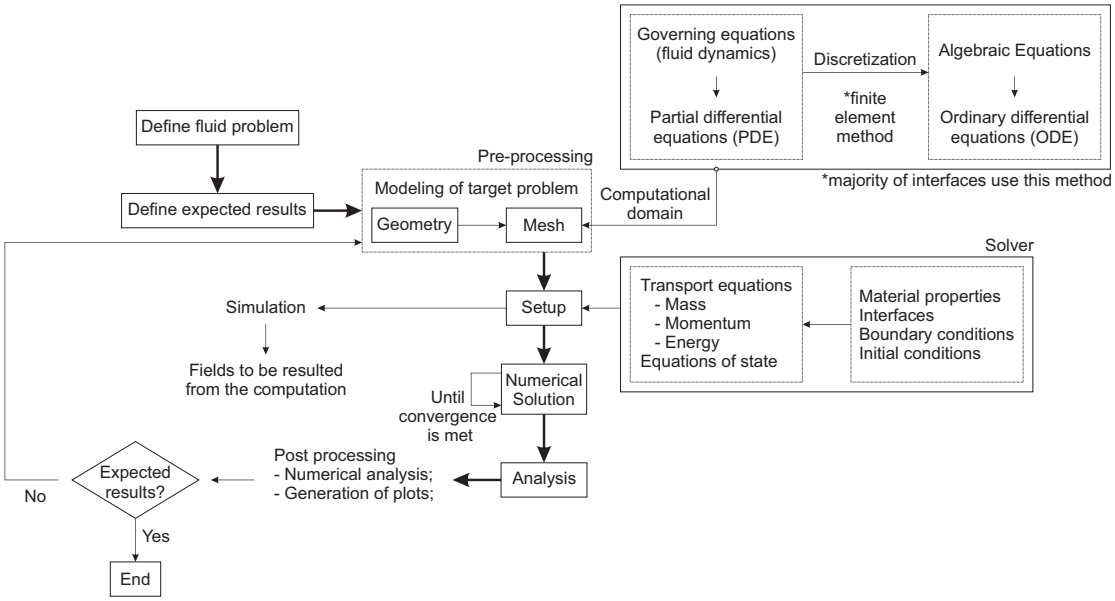

Fig. 3.1 A typical workflow CFD for calculations.

In order to describe the physical properties, mathematical equations have to be used. The basis of all CFD simulations is represented by the Navier-Stokes governing

equations. These equations define the three conservation laws and state that in a closed system: mass, momentum and energy are conserved.

Fig. 3.1 shows a typical CFD workflow. The preprocessing part implies realizing the CAD (Computer Aided-Design) from which a mesh, needed for the calculations, can be realized. The governing equations in their analytical form pass through a discretization process from which the algebraic equations are obtained. The latter can then be used by a computer code to solve the fluid problem.

3.2 Overview of the HADO-CSC CFD simulations

One first step in solving the HADO-CSC fluid flow problem has been to validate the simulation solutions against the analythical solutions available in the case of a quasi-one-dimensional flow. For the latter, the area change is the cause for the variation in the flow properties as a function of the x coordinate along the nozzle, as seen in Fig. 3.2.

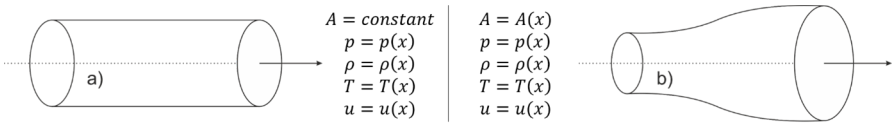

Fig. 3.2 Flow variables in a straight cylindrical nozzle (a) and converging-diverging nozzle (b).

The flow properties are assumed to be uniform across any cross section of area A, with the values dictated by the central line.

3.3 Isentropic flow regime

If the flow through a nozzle is gradually compressed (area decreases) and then gradually expanded (area increases), the flow conditions return to their original values. Such a process is reversible. From a consideration of the second law of thermodynamics, a reversible flow maintains a constant value of entropy. This type of flow is isentropic, occurring when the change in flow variables is small and gradual such as the ideal flow through the nozzle.

A flow is considered supersonic when the Mach number (ratio of flow velocity over the speed of sound in that medium) is above a value of one. Converging-diverging nozzles, also known as Laval nozzles, have been firstly considered as the transportation mechanism for the created ions as this type of nozzle is mainly used to accelerate gases into supersonic jets.

The characteristics of the transitioning from a subsonic to a supersonic flow regime in a Laval nozzle, can be described in a quasi-one-dimensional symmetry with the change

in velocity being expressed in terms of the Mach number M by the area-velocity relation:

$$\frac{dA}{A} = (M^2 - 1)\frac{dv}{v} \tag{3.1}$$

where v represents the velocity of the gas and A the area of the enclosing structure.

Equation 3.1, under the assumption of a callorically perfect gas, can be explicitely solved to obtain the Area-Mach number equation:

$$\left(\frac{A}{A_t}\right)^2 = \frac{1}{M^2}\left[\frac{2}{\gamma+1}\left(1+\frac{\gamma-1}{2}M^2\right)\right]^{\frac{\gamma+1}{\gamma-1}} \tag{3.2}$$

where A_t is the nozzle throat area that must be smaller than A to have a physical meaning, and $\gamma = c_p/c_v$. For every value of A, larger than the throat area A_t, two real solutions fulfill eq. 3.2, corresponding to a subsonic value and a supersonic value, as seen in the two plots of Figure 3.3.

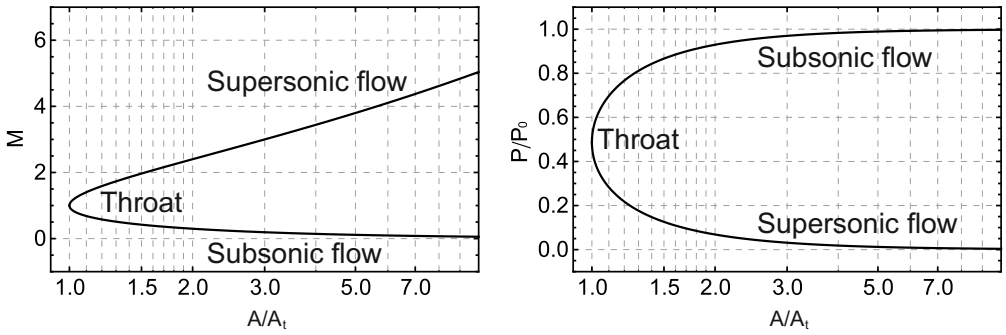

Fig. 3.3 Gas Mach number transitioning from a subsonic to a supersonic state as a function of the area ratio (left); Pressure ratio as a function of area ratio in the transition from a subsonic to a supersonic flow (right).

3.4 CFD simulations of a Laval nozzle

The current gas cell is meant to use helium gas at 70-80 K and 200-300 mbar, which can be considered with a very good approximation a calorically perfect gas. Although, there exist significant heat sources, represented by the RF fields of the HADO-CSC, they can be neglected in the regions inside and around the nozzles, where the CFD simulations are performed. Hence the flow inside the gas jets is adiabatic.

The fluid dynamics simulations have been performed using COMSOL Multiphysics©, specifically the High Mach Number Flow module [19].

The Laval nozzle has been first simulated by defining the inlet and outlet pressure boundaries of 300 mbar for the inlet and 3 mbar for the outlet, corresponding to the two chamber pressures of the HADO-CSC. The overall results are emphasized in Fig. 3.4. The simulation results are shown in Fig. 3.5 and were determined by considering the

values along the nozzle centreline. The gas jet indeed reaches the expected isentropic values at the throat, namely $M = 1$, $P/P_0 = 0.49$, $T/T_0 = 0.75$.

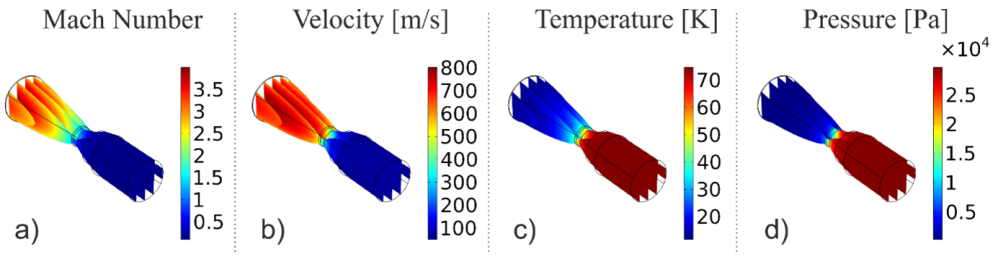

Fig. 3.4 Mach number (a), velocity (b), temperature (c), pressure (d).

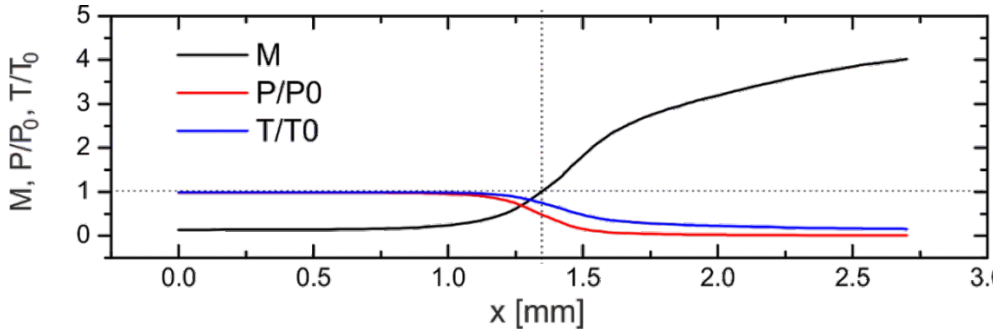

Fig. 3.5 (top) Dependence on distance x along the nozzle axis of the Mach number, total to static ratios of pressure and temperature. Dashed line shows the throat location.

At the outlet, a Mach number of $M_{out} = 4.03$ is obtained, which is within 0.25% of the analytic value. This value is a combination of the acceleration to $u_{out} = 805$ m/s with a temperature drop to $T_{out} = 11.5$ K.

For $M_{out} = 4.03$ and $P_0 = 300$ mbar, an outlet pressure of $P_{out} = 3$ mbar is needed to reach an isentropic flow. A higher value of the pressure ratio will lead to the formation of a shock in the divergent region. Fig. 3.6 presents the 3 mbar case discussed above and one in which the outlet pressure has been modified drastically (200 mbar).

Since the backpressure downstream the nozzle is governed independently, pressure differences lead to the formation of shocks, either at the exit of the nozzle or a normal shock somewhere in the divergent section. These lead to a quick Mach number drop and a big rise of P/P_0 and T/T_0.

If the back pressure is too high, normal shocks form in the divergent part of the nozzle. This type of shocks is a potential problem because they generate vibrations in the CSC wall and because the flow discontinuities that they generate can affect the transport of the heavy ions.

3.4.1 Normal shocks in a Laval nozzle

When an object moves faster than the speed of sound, and there is an abrupt decrease in the flow area, the flow process is considered irreversible leading to an entropy increase

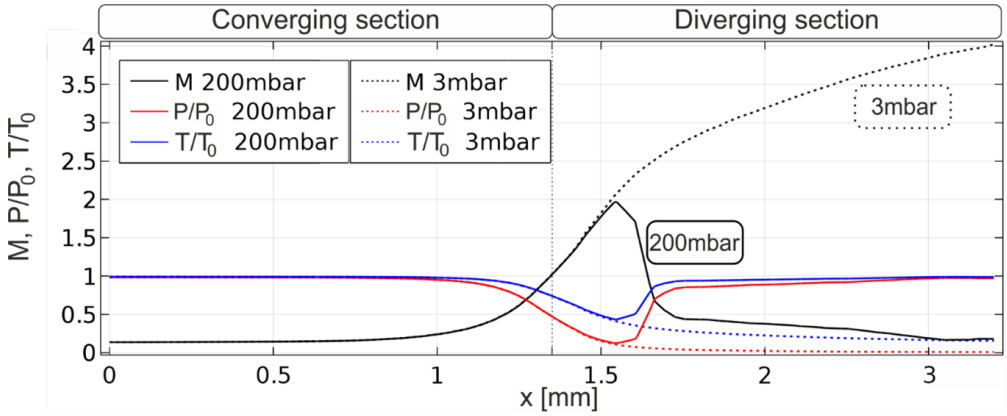

Fig. 3.6 Dependence on the distance x, for an input pressure of 300 mbar, along the nozzle axis of the Mach number and total to static ratios for pressure and temperature; 200 mbar at outlet (solid lines) and 3 mbar at outlet (dotted lines).

and shock waves are generated [20]. The effects that lead to this increase are viscosity and thermal conduction. These shock waves are very small regions in the gas where the properties change by a large amount. Across this shock wave, the total pressure, temperature and gas density increase almost instantly. Moreover, if the shock wave is perpendicular to the flow direction it is called a normal shock. This type of shock appears in the divergent section of the nozzle.

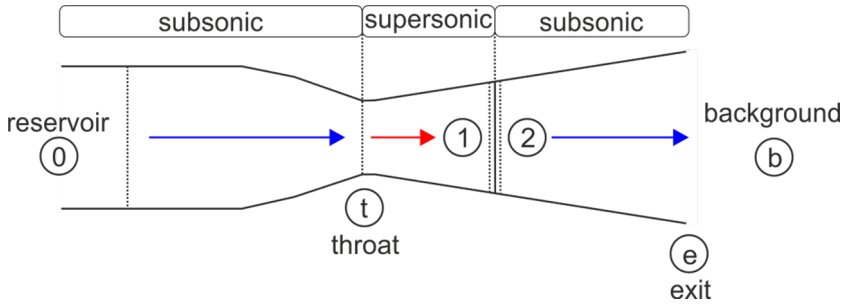

Fig. 3.7 Schematic representation of the pressure in a converging-diverging nozzle with a normal shock in the diverging section. A_t = throat area of nozzle, A_{NS} = Normal shock area, A_1^* = sonic area upstream the shock wave, A_2^* = sonic area downstream the shock wave.

A MATLAB code was written and used to output directly the normal shock location based on an iterative method i.e., the bisection method. The results are summarized in table 3.1 and is compared to the simulation results. The exit to throat ratio has been calculated by interpolating the data from Fig. 3.3 using the normal shock location.

As it can be seen, the simulated location is close to the theoretical one. In the Mach number there is a certain discrepancy that arises from the small location difference.

3.4.2 Heat Addition Influence

In the thesis the heat addition influence is briefly described.

Table 3.1 Comparison between theoretical and simulation results for a 300 - 200 mbar pressure drop.

Parameter	**Theoretical**	**Simulation**	**Error [%]**
$\left(\frac{A_e}{A_t}\right)_{NS}$	1.7691	1.6881	4.79
M_{NS}	2.22	1.9696	12.7
Location [mm]	1.5701	1.548	1.42

3.4.3 Friction influence

The influence of friction is briefly described. The included table in the thesis presents the influence of heat and friction on helium flows.

3.5 Demonstrator Unit using Laval nozzles : CFD simulations

So far, the simulations of jets in Laval nozzles have proven that the fluid model is within acceptable parameters when compared to the theoretical isentropic solutions. Moreover, as exemplified in Fig. 3.6 a pressure ratio different than the isentropic condition leads to the formation of shockwaves.

The actual application of the Laval nozzle is to help the fission products pass from the stopping chamber to the extraction chamber, thus acting like an ion guide. The particles are transported to the nozzle inlet by RF carpets (concentric electrodes on which RF and radial DC fields are applied) that guide the ions towards the nozzle inlet and DC fields applied on the chamber electrodes to further help the particle trajectories. As RF carpets are not the subject of the current work, they have been designed simply by large cylinders with the Laval nozzle presented earlier, in the middle.

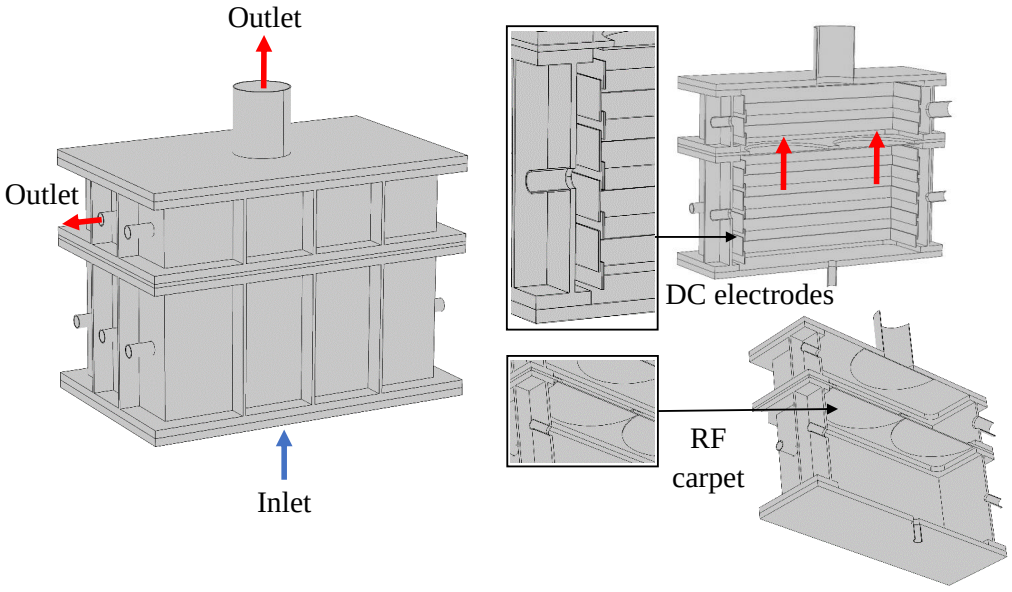

Fig. 3.8 HADO-CSC prototype (Demo-CSC) used to for the initial testing (left); section to see the RF carpets and DC electrodes (right).

The design showed in Fig. 3.8 represents a demonstrator unit, a smaller HADO-CSC with only two nozzles considered. CFD simulations require a great deal of computing power, hence the considered geometry was a section of the complete chamber on which a symmetry operation was used for further postprocessing the jet in the chamber.

As the DC electrodes inside the chamber do not influence greatly the jets and fluid flow, they have been removed and only the RF carpets that make the actual nozzles were left. Also, the interior volume that forms the fluid volume in which the physics is applied has been built with COMSOL Multiphysics.

The used material was also helium with the same properties as in the case of the Laval nozzle.

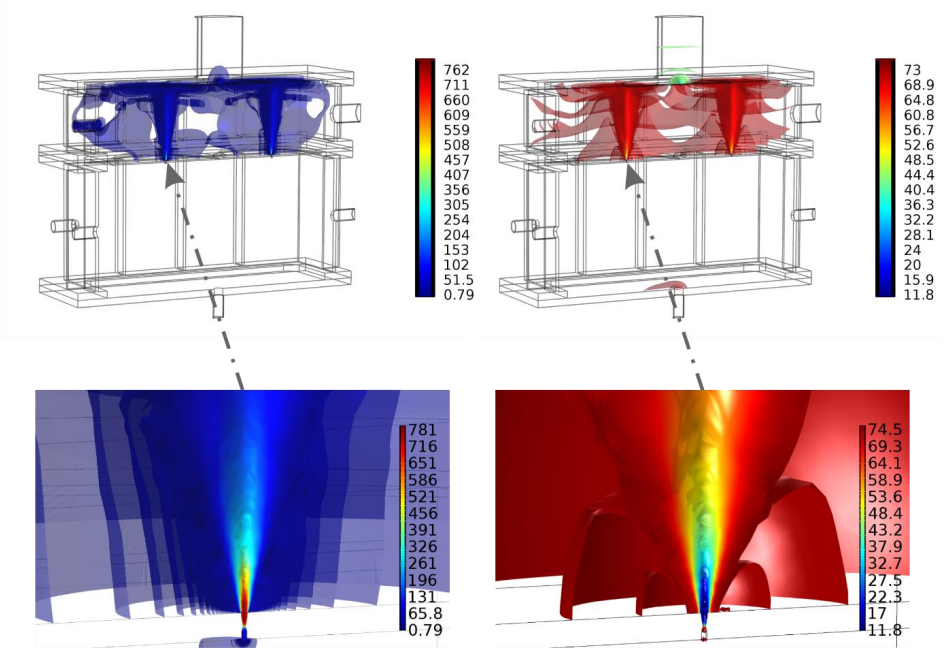

Fig. 3.9 Velocity isosurface (left) and temperature isosurface (right) of the formed supersonic jet in the gas cell with two Laval nozzles with their corresponding color legends.

The supersonic gas jets formed with the Laval when they are used as the ion guide inside the gas cell are presented in Fig. 3.9, where the nozzle is placed between the stopping chamber and the extraction chamber. The height is 10 cm.

Fig. 3.10 shows the velocity, temperature and pressure distributions along the nozzle and also 2 mm before and after it. The simulation program takes into consideration turbulences, compression and expansion effects. Since the jet is slightly under expanded at the exit, expansion waves are still possible leading to a second Mach peak as seen in Fig. 3.10. This under expansion leads to the decrease in the exit Mach number by 5% when compared to the isentropic solution. The exit flow velocity is 792 m/s corresponding to M = 3.81 at a temperature of 12.45 K and a pressure of 3.01 mbar.

Mass conservation between the inlet and the outlet of the CSC is validated with a relative error of 0.7%. The mass has been calculated using eq. 3.3.

$$\dot{m} = \iint_A \rho \cdot v \, dA \tag{3.3}$$

where m - mass flow rate, v - flow velocity acting on the surface, A - considered surface, ρ - fluid density.

The same study, as done before for Fig. 3.5 has been iterated here. The Mach number 2 mm before and after the nozzle as well as T/T_0, P/P_0 distributions are shown in Fig. 3.10.

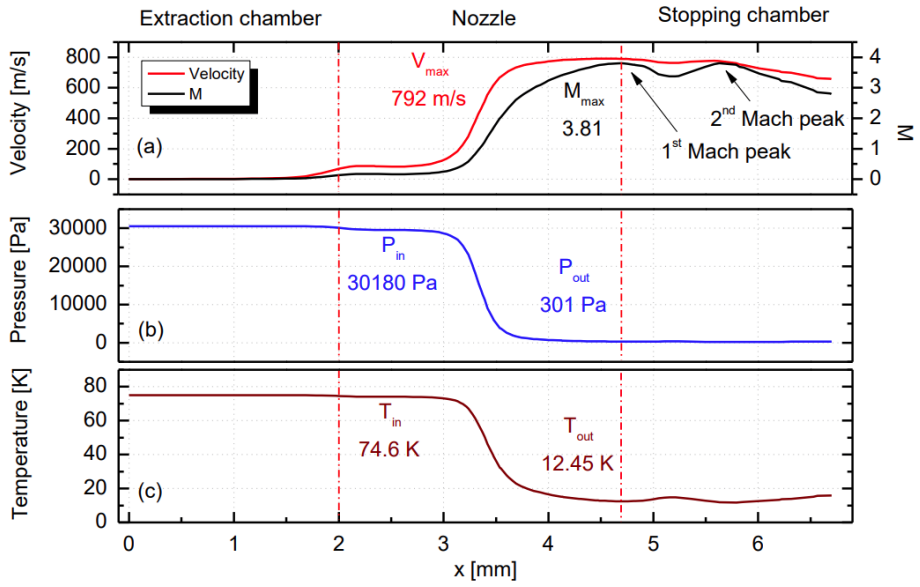

Fig. 3.10 a)Velocity, Mach number, b) temperature and c) pressure distributions covering the nozzle and 2 mm before and after it. The dashed lines indicate the inlet and outlet of the Laval nozzle.

Table 3.2 shows the theoretical and simulated values for $M, P/P_0, T/T_0$ at the nozzle throat and for M at the nozzle outlet.

Table 3.2 Comparison between theoretical and simulated values for the convergent-divergent nozzle in the Demo-CSC.

Parameter	**Theoretical**	**Simulation**	**Relative Error** [%]
M_{throat}	1	1.02	1.96
$P/P_{0-throat}$	0.487	0.474	2.74
$T/T_{0-throat}$	0.75	0.7425	1.01
$M_{outlet-supersonic}$	4.035	3.802	6.13

3.6 Ion extraction from gas cells with supersonic jets formed in Laval nozzles

A time dependent study has been performed covering 2 ms with a time step of 0.1 ms. Representative isotopes for the above two regions have been considered, namely ^{89}Rb and ^{145}Ce. Fig. 3.11 shows the particle behavior in the nozzle. In 20 µs all isotopes reach the nozzle outlet and tend to reach the maximum velocity of 792 m/s.

The ions follow the gas flow streamlines which converge towards the throat. The maximum velocity is met at the nozzle centre and it decreases towards the boundary surface. This can be seen in the phase portrait in the bottom right of Fig. 3.11.

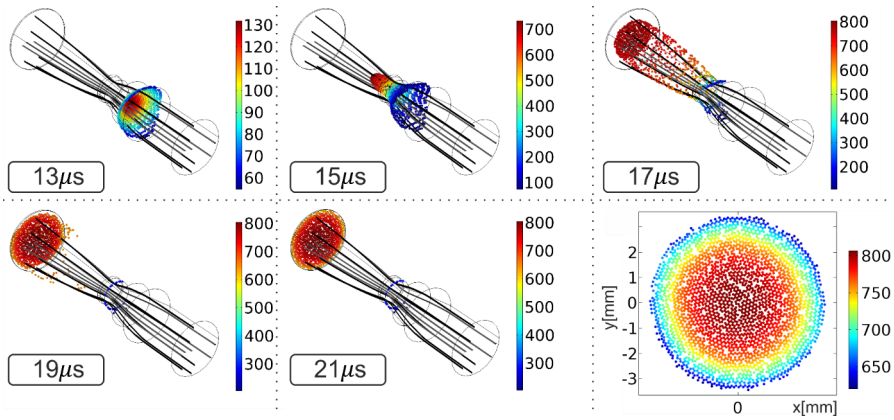

Fig. 3.11 Drift velocity distributions in [m/s] for a thousand ^{145}Ce ions at different time steps and phase portrait describing the particle positions at the outlet, color coded by their velocity.

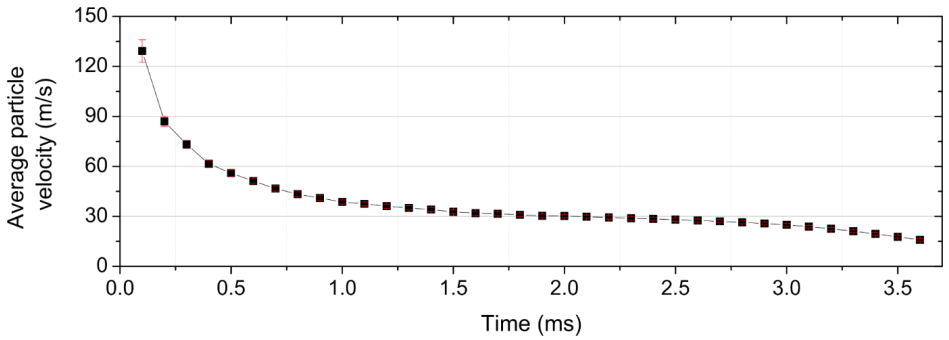

Fig. 3.12 Average particle velocity for ^{145}Ce in the Demo-CSC in function of time.

The average particle velocity in function of time for ^{145}Ce has been plotted in Fig. 3.12 covering the 10 cm of the extraction chamber. The ions reach the RF carpet on the upper wall of the extraction chamber in 1.9 ms at an average velocity of 10.2 m/s. The transport times can be decreased by an order of magnitude with the electrical fields.

3.7 Summary of chapter 3

A short overview and summary of the chapter is provided in the thesis. This also emphasizes the original work of the author.

Chapter 4

HADO-CSC - Gas system design

4.1 Helium Recovery Unit - Overview

This gas cell design with an orthogonal extraction considers two chambers (Fig. 2.4). This is highly dependent on the gas jets to guide the fission products. These jets exhibit different behaviors when experiencing changes in the pressure conditions in both chambers. The system meant to deal with the stable gas operation of the HADO-CSC is the Helium Recovery Unit (HRU). This is a cost-effective system, meant to be used for the recirculation of helium gas, used in conjunction with the HADO-CSC.

Cleanliness in the HADO-CSC is very important as impurities can neutralize the charged fission products. As such, Ultra-High Vacuum (UHV) components are meant to be used. In additions to this, all flanges provide CF-F and VCR connections. The required quantity of gas that the system is capable of re-compressing is considered to be 2 m^3/h. The system includes two buffer vessels: one over-pressure vessel ($\approx$ 4 bar, 250 l) and one under-pressure or vacuum vessel ($\approx$ 0.8 bar, 150 l).

The HRU is briefly described in the current summary and follows the same structure as in the thesis.

4.2 System specifications

The overall specifications of the HRU and its performance are directly connected to the HADO-CSC parameters which are detailed in the thesis.

A flow value of $\approx$ 2.9 l/min (STU measurements - chapter 5) at RT for a 300 – 10 mbar pressure drop using a nozzle with a length of 1.1 mm, leads for 8 RF carpets to an approx. value of 23.2 l/min which is slightly less than the 2 m^3/h that is considered for the system. The leakage rate of all components in the HRU have been chosen to provide a value less than 10^{-5} mbar·l/s. The overall percentage of recovered helium of purity 6.0 when designing the system has been considered to be $\approx$ 98%. The purity of the gas will be improved also by the use of purifiers along the gas lines. The HRU system consists

of several parts or modules. The smaller parts are meant to be assembled and then be integrated in the bigger frame of the HRU. All components are discussed in detail in the thesis.

4.3 Gas supply system

Gas systems used in nuclear physics experiments typically use pressurized bottles filled with the respective gas at hundreds of Bar. Typically, gas bottles of 50 l, 200 Bar are used. This is also the case for the HRU. A pressure regulator, placed on the helium bottle will limit the input pressure of the HRU to a pressure between 4 - 10 Bar. This pressure will be chosen according to the control valve that is used at the inlet of the HRU to finely adjust the pressure in the first chamber of interest.

The supply of fresh helium gas is regulated by a Mass Flow Controller (MFC) mounted at the inlet of the HRU. This MFC provides 50 slm/min and has two important functions: it acts as a control valve which finely compensates the losses through the system and can monitor the actual flow, hence an estimation of the system losses can be expressed.

4.4 Vacuum pumping system at the inlet of HRU

The pumping system that covers the exit of the Extraction Chamber (inlet of HRU) consists of an assembly of two pumps: an Adixen A100L which is fitted with a booster pump, type Pfeifer OKTA 250M.

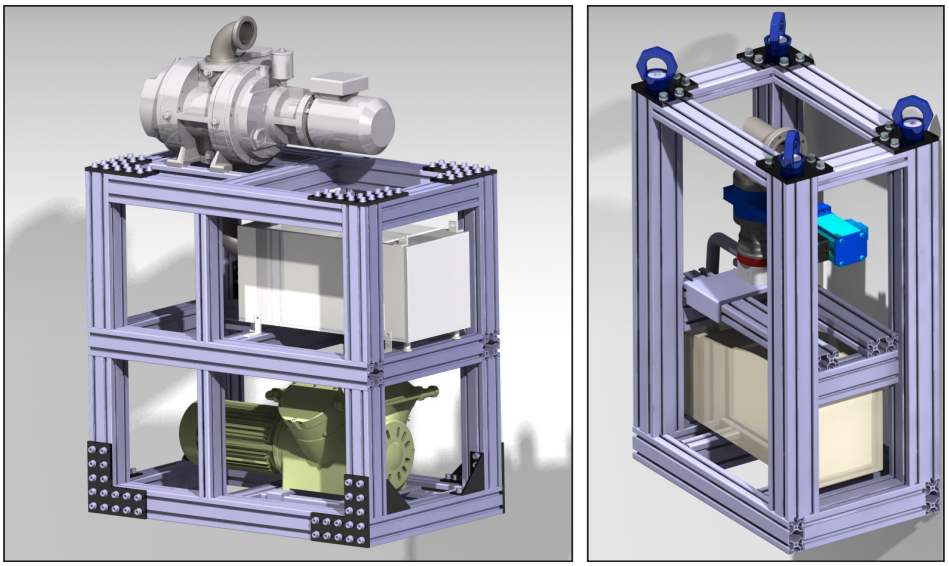

Fig. 4.1 3D Renders of Pfeifer OKTA 250M (top), ADIXEN A100L (middle), KNF1400 Compressor (bottom) sub-assembly.

Fig.4.1 (left) shows the sub-assembly for the three considered pumps that form the vacuum sub-assembly. This comes as an advantage when building up the complete setup as smaller sub-sections of the HRU can be assembled and later-on craned down. This lowers the install time and possible maintenance procedures.

4.5 Compressor unit with vacuum and pressure receivers.

The membrane compressor unit is used for re-pressurizing the pre-pressurized helium gas by the Adixen A100L – OKTA 250M configuration. It is based on a KNF N1400 series with a motor that is suitable for frequency converter operation and a leak rate less than $1 \cdot 10^{-6}$ mbar l/s.

The compressor is fitted with appropriately chosen buffer vessels, mounted before (vacuum vessel) and after the compressor (Pressure vessel), thus they act as a buffer between the compressor and the fluctuating pressure. The two vessels assure the system stability and minimize the compressor loading and unloading cycles which strongly depend on the demand fluctuations.

A regular 50-liter Helium bottle at a pressure of 200 Bar has a gas volume at atmospheric pressure of 10000 liters of Helium, translated to approx. 1.78 kg of Helium.

One helium bottle will be able to fill the HADO-CSC and the HRU components $\approx$ 5 times. Moreover, at a loss of 33 mg/min (the leak rate of the other components is considered less than $1 \cdot 10^{-5}$ mbar l/s and thus negligible) the system will be capable of operating continuously for more than a month (37 days at highest pressure) before having to change the helium bottle. Moreover, the two vessels will be also connected to the vacuum port for a quick venting procedure with two manual valves, with a diameter of DN25. These are manual as this procedure is performed only when starting the system.

4.6 Pumping system for vacuum and gas exhaust.

The vacuum system consists of a HiPace 80 turbopump with a DN 63 CF-F top connector offering a 2.7 mbar l/s maximum gas throughput for He.

This part of the HRU is meant to allow a fast pump-down of the HRU and the connecting tubing before starting the filling procedure. A pressure of less than $10^{-}5$ mbar should be reached, before starting the filling with He gas, to ensure negligible amount of contamination to the He gas.

Figure 4.1 (right) shows the sub-frame used to hold the two pumps, which will be mounted and later-on craned down into the HRU frame.

4.7 Purifying System

There are active and passive purifiers meant to be installed in the HRU to increase the He gas quality. One can select between the active and the passive getter by choosing the correct path by closing and opening the correct valves. As these getters do not come with remote controlled valves, before and after the manual valves for each purifier, solenoid valves will be used

Furthermore, after the two getters, there is in the HRU another smaller getter used for introducing trace gases (cleaned afterwards by the small passive getter), in the stopping gas to control the charge state of the extracted ions. This operation is performed using a Pfeiffer UDV146 all-metal regulating valve (controlled by an RVG050 controller) with a flow ranging from 0 – 1 ln/min. Fig. 4.2 (right) shows the gas panel of the HRU on which all the input and output connections are located.

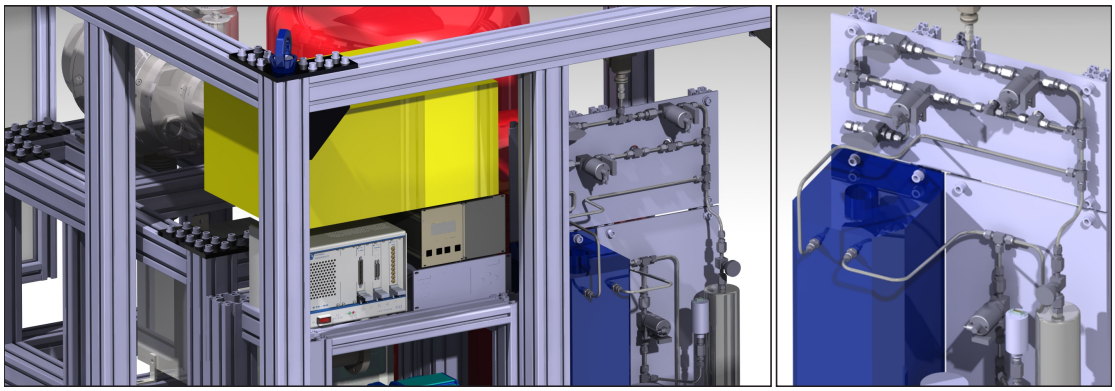

Fig. 4.2 (**Left panel**)PXI 1073 chassis placement (left). DCU110, RVC300, MKS946 (Right). The yellow box (250 x 350 x 520 mm) is the space required for electrical connections, wiring, DIN rails, terminal and distribution blocks and all PXI accessories. (**Right panel**) HRU gas panel with input and output connections. The active getter is represented in blue and the passive getter with grey.

All gas components are fixed on the two 5 mm plates, i.e., required tees, crosses, and solenoid valves. The connection between the getters and the fixed components is done by flexible stainless steel 316L 1/4' tubing.

4.8 Control System

The control system of the entire HRU consists of two subsystems: the hardware (further named as the command system or CS) and software (further named as the command console or CC). Furthermore, this represents a closed-loop control system. By considering the current CSC at the FRS Ion Catcher at GSI for which the slow control has proven to work particularly good with LabVIEW the desired programming will be done using it. For this the Actor Framework will be used with current CSPP (Control System++)

libraries and utilities. Chapter 6 treats in detail the CSPP architecture and the current slow control implementation of the FRS Ion Catcher.

The command system is an integral part of the HRU that can monitor all the equipment parameters and with the help of the command console can control the different subsystems automatically on a pre-programmed algorithm.

The command system is based on a NI-PXI chassis, specifically designed to work in such applications. The chosen chassis, namely NI PXIe-1073 can accommodate 5-slot PXI modules: 3 Hybrid Slots and 2 PXI Express Slots, with a 250 MB/s bandwidth and one controller module. The chassis is responsible for providing the DC power to the CompactPCI/PXI backplane from a single 100 – 240 VAC input voltage.

The command console is based on LabVIEW as the main programming language. This has proven to perform particularly good at the present FRS Ion Catcher slow control and is a worldwide used solution. The chosen architecture will be based on the Actor Framework which utilizes the CSPP tools and utilities developed at GSI. The main advantage of this architecture is the usage of shared variables across the network and makes it easy to implement it in the future CSC control system.

4.9 Mechanical Design

The outer frame of the HRU, in which all the sub-assemblies will be mounted, is emphasized in Fig. 4.3. The overall resistance in terms of mechanical stress is provided by the 15 mm in width strengthened aluminum “L” shaped corners and joint corners. The casters can sustain 1 tone. There are four swivel eye nuts on the top part, type RSC2016, each having a max. load of 1.5 tone. The frame requires approx. 30 m of Al profiles (150 Kg) and leads to a total frame weight of approx. 200 kg with all panels mounted. Moreover, the total weight of the entire HRU system is less than 1.2 tone.

Furthermore, to increase the overall stiffness of all assemblies, automatic connectors will be used. Hex head cap screws will be used instead of socket cap screws to avoid any dead time that could arise from rounded socket caps. Moreover, the outer frame will be constructed out of full profiles with the sub-assemblies constructed with hollow profiles. In the latter case, of the smaller assemblies this is possible as the weight does not exceed 300 Kg.

The assembly of the HRU can either start by building just the base of the HRU outer frame, install the sub-assemblies and then add the rest of the outer frame components or build the entire outer frame and crane down all sub-assemblies from the top of the HRU. The complete mechanical design of the entire HRU is emphasized in Fig. 4.3.

Furthermore, the HRU frame will be closed with a pair of panels on each side. These are constructed out of 40 x 40 mm aluminum frames with either Plexiglas or metal sheets. The estimated heat generation in the closed system is a few kW due mainly to

Fig. 4.3 HRU outer frame on which the sub-assemblies are mounted.

the dissipated heat by the pump motors. For 4.5 kW a required air flow of 48.3 m^3 was calculated, for a temperature difference of 5°C.

Chapter 4 has treated in detail the design stage of the Helium Recovery Unit. Such a setup is of utmost importance when coupled with the HADO-CSC as it reduces the cost of use, primarily of the Helium gas and minimizes the overall maintenance time due to its modular design.

The original work is emphasized by the conceptualization of the system, mechanical design, working gas diagrams and logical diagrams. It is based on the internal report submitted to the FRS-IC group entitled: *Helium Recovery Unit for the LEB CSC*, A.State and T. Dickel.

4.10 Summary of chapter 4

A short overview and summary of the chapter is provided in the thesis. This also emphasizes the original work of the author.

Chapter 5

The Supersonic Test Unit - characterizing gas jets experimentally

5.1 Overview

A characterization setup, i.e., the Supersonic Test Unit (STU), using the same pressure values as the HADO-CSC has been designed and built for several studies to be first tested at room temperature. Different characterization techniques have been envisaged, both optical and direct measurements, e.g. Schlieren imaging, gas jet fluorescence, Pitot tube measurements.

5.1.1 Design

The Supersonic Test Unit (STU) has been designed, constructed and used to serve as a prototype setup for characterization methods of supersonic jets. Its modular design makes it suitable for a wide range of measurements at room temperature. The design and construction were done having in mind modularity, so changing from one method to another is done with minimal effort. The 3D renders of the overall design are showed in Fig. 5.1. Due to the transparent construction of the chamber, optical methods can be also used. As such, the Schlieren optical method which relies on the changes in the refractive index of a beam of light passing though a density gradient (induced by the jet) was tested. Both a white LED with a changeable brightness and a HeNe laser were used. These provide good results in high density gradients but the method is not sensitive enough to capture any changes in density resulted from the STU jets.

An optical method to visualize the jet that emerges in the second acrylic chamber, that mimics the extraction chamber conditions of the CSC, is the gas jet fluorescence technique. By the use of a single needle electrode placed inside the nozzle before the nozzle output, connected to a HV power supply (CAEN 8 kV), the emerging gas exhibits a visible glow. An 1 MΩ resistor was used for the input to limit the current. At around 300 to 400 V a discharge is initiated. In the presence of a flow of gas, the resulting

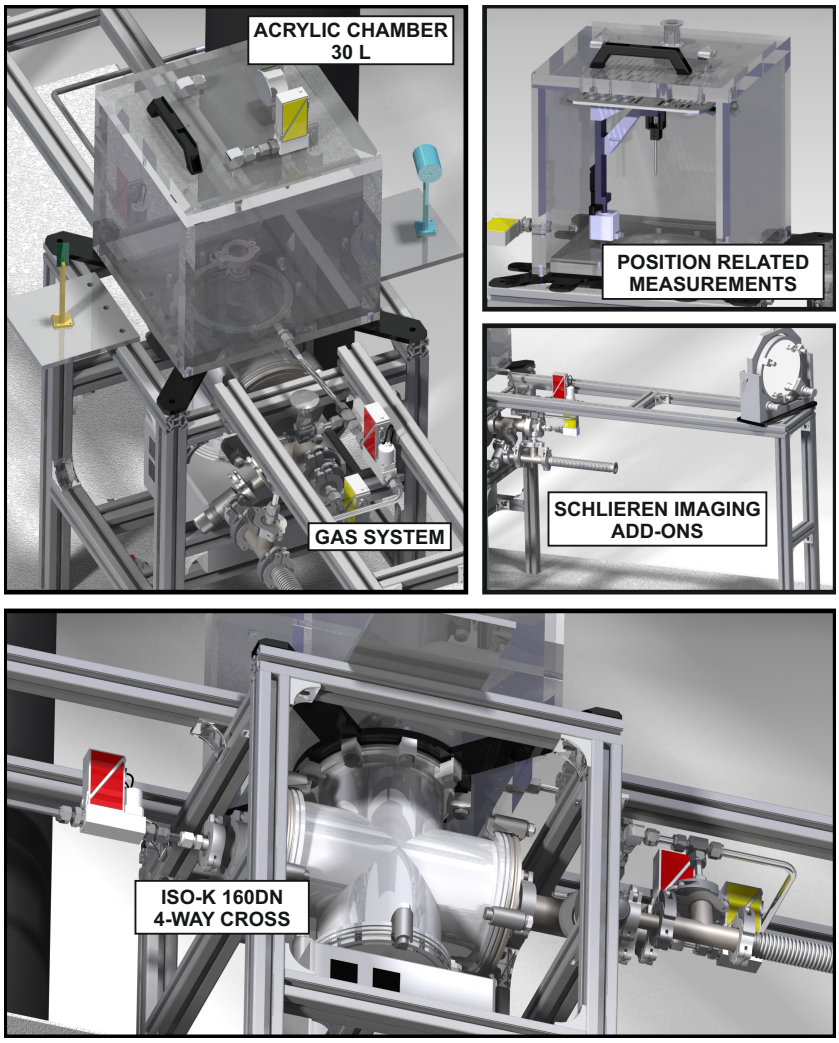

Fig. 5.1 3D renders of the complete STU mechanical design. Different add-ons can be seen, for different measurement methods, i.e., position related measurements or for Schlieren imaging.

flow that expands in the acrylic chamber exhibits a glow corresponding to the relaxation towards the ground state of the constituent atoms that form the gas, previously exited by the arc discharge. The schematic representation of the used setup is depicted in Fig. 5.2 top.

5.1.2 Gas System

The STU gas system and all its components that can mimic the HADO-CSC pressure drop, at room temperature are described in detail.

5.1.3 Control System

The control system has been developed in LabVIEW using a state machine architecture.

5.2 Measurement Methods

Different approaches and methods for characterizing the jets were taken into consideration: Gas jet fluorescence, Pitot tube measurements, Schlieren imaging.

5.2.1 Gas jet Fluorescence

5.2.2 Methodology

The gas jet fluorescence technique has been successfully used to describe the behavior of the jets when modifying the two important pressures of the gas cell: the backing pressure and the background pressure. While using this method different sub-mm nozzle diameters have been investigated. These have indicated that the jets in all cases follow a strongly under-expanded scenario with a repeated shock-wave pattern. The simulations are in good agreement with the mass flow rates measured with the STU and the formation of the first normal shock. The mesh size will be addressed in order to correlate even better with the real jets.

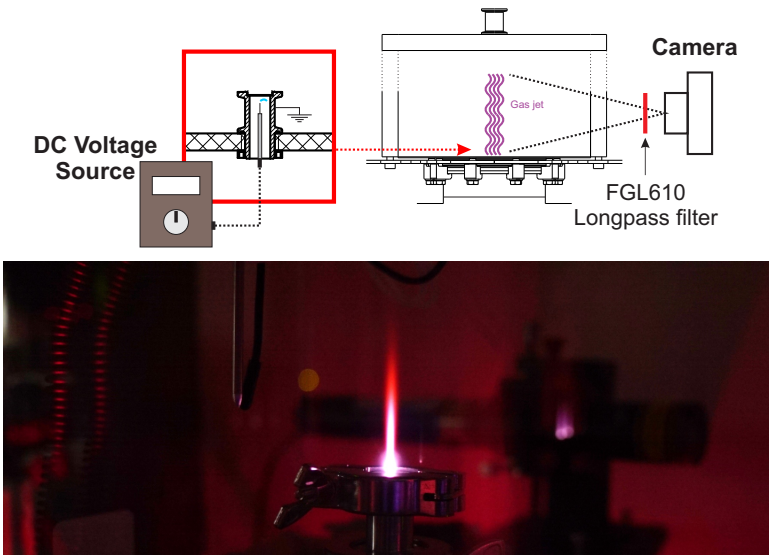

Fig. 5.2 (Top) Schematic representation of the setup used for the gas jet fluorescence experiment. (Bottom) Picture of the emerging gas from a 0.7 mm nozzle at a pressure difference of 200 - 10 mbar. Picture taken without the filter attached to the camera. A sensitivity of ISO-1600, an exposure time of 3.2 sec. and an f-stop of f/2.8 were used on a SONY alpha a7s ILCE7SM2/B 12.2 MP on which SEL2470GM FE 24-70 mm F2.8 G Master Full Frame Zoom Lens was mounted.

5.2.3 Pressure effects

Three cylindrical nozzles, 0.5 mm, 0.7 mm and 0.9 mm with a length of 1.1 mm were used. Although the results using the fluorescence technique are more on the qualitative

side, several behaviors can be expressed. Two important parameters for any gas cell that uses jets as a guiding mechanism, are the two pressures that form the jet, i.e., the backing pressure and the background pressure. As such, the behavior when modifying each of the two pressures has been investigated.

5.2.4 Shock waves

The shock wave pattern of the under-expanded jets has been compared to the simulations. The location of the first shock wave is in agreement to the CFD simulations.

5.2.5 Pitot tube measurements

A second measurement that was performed implied using a Pitot tube. The latter represents a flow measurement device with which one can measure the total and static pressures along the jet axis. By doing this, pressure profiles along the jet axis can be done and under certain assumptions velocity can be approximated using Bernoulli's equation. The latter, requires the assumption of an inviscid, incompressible flow and by knowing the difference between the two pressures and the flow density at the tip of the Pitot tube one can approximate velocity. In order to have repetitive and accurate measurements a moving system was constructed. This is based on two high-precision linear stages which were fitted with stepper motors. The motors are used in full-step mode being driven by small drivers placed on a small development board that is controlled via LabVIEW.

Two modes of operation are intended to be used with the current setup. An XY mode which can be used for mapping and an XZ mode which can be used for performing axial measurements. The space restrictions inside the chamber lead to a coverage of the pressure along the jet axis of only 6.2 cm. As such, a 0.5 mm nozzle was used. This nozzle diameter was selected as higher diameters lead to higher velocities. This statement is assumed based on the gas jet fluorescence measurements which provide more jet intensity in regions close to the Pitot tube position as one increases the nozzle diameter. Moreover, the 0.5 mm nozzle does not present an observed bow shock (curved normal shock) forming at the tip of the Pitot tube. This behavior would be an indicator that the jet has a high Mach number and the total pressure measured by the Pitot tube is not the one that is desired, and one would measure the pressure behind a normal shock which would indicate a smaller pressure value. A pressure difference $P_{tot} - P_{st}$ of 0.2 mbar which is found at 6.2 cm would translate to a velocity of $\approx$ 150 m/s at a gas density of 0.00215 kg/m^3. The latter density is considered from the NIST database of thermodynamic properties of Helium at 12.2 mbar and 18°C. The temperature has been measured using a PT100 placed inside the chamber right at the tip of the Pitot tube. The used absolute pressure sensors is prone to very large errors due to the accuracy of the used pressure sensors of $\pm$2.5 mbar. Moreover, a variation of $\pm$0.25 mbar leads to a variation in velocity of $\pm$75 m/s. The static pressure does not have a strong change,

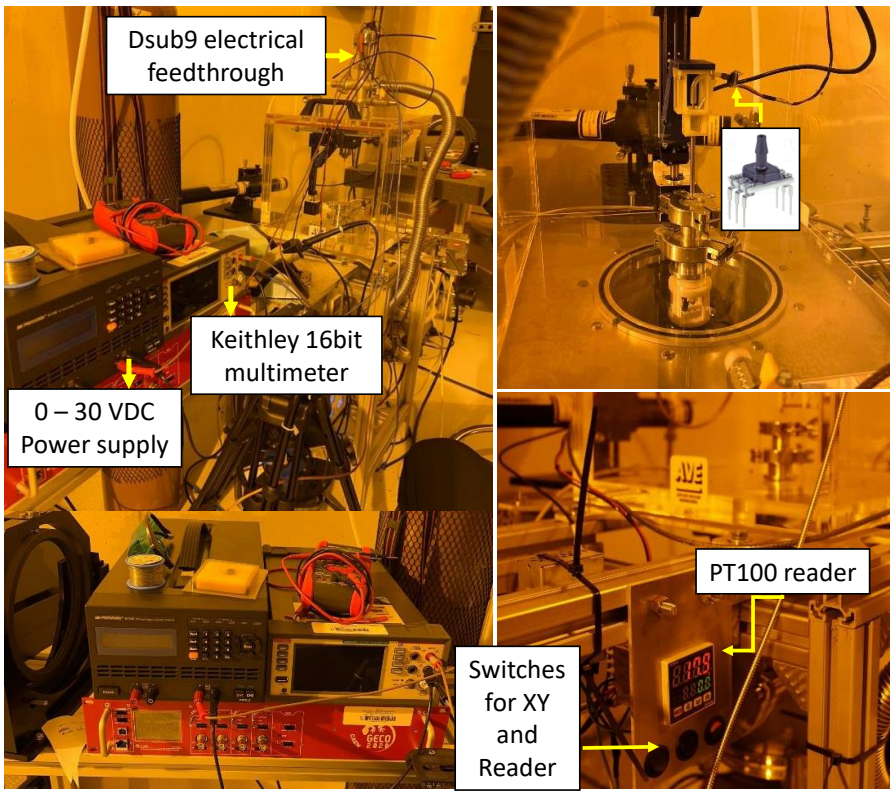

Fig. 5.3 Pictures of the actual STU and equipment used for doing the pressure profiles along the jet axis.

leading to just 1 mbar variation from the nozzle outlet to the maximum point at which the setup can be used. As such, only the total pressure is the one that is important to be known. Based on the measured pressure along the 6.2 cm and extrapolating, after ≈ 1 cm the total pressure would match the static pressure. This indicates a small pressure difference which in turn leads to a low velocity, as seen in the simulation results.

5.2.6 Schlieren imaging

One proposed method for the current experimental setup was a double Schlieren imaging technique. This method relies on the fact that light rays when passing through a medium characterized by a density gradient are distorted due to the variations in the refractive index.

5.3 Computational fluid dynamics simulations

CFD simulations have been performed for different nozzle diameters at the same pressure difference.

5.4 Flow measurements

The required mass flow rate through the system for each nozzle diameter in order to maintain different pressure differences has been measured with the STU.

5.5 Summary of Chapter 5

This section presents the summary of the chapter and future measurements with the STU.

The results described in the current chapter are in advanced preparation to be submitted to a peer-reviewed journal with the following title: *Methods of characterization of supersonic helium jets in cylindrical nozzles used for ion beam transport*, A. N. State, D. L. Balabanski, P. Constantin, M. Cuciuc, P. Ghenuche, D. Nichita, A. Rotaru, A. Spataru.

Chapter 6

Slow control systems used for nuclear physics in LabVIEW

6.1 Introduction

Chapter 6 is focused on two control systems, programmed in LabVIEW, with different design approaches, used in nuclear physics.

6.2 Control system based on QMH in LabVIEW - automation of the 4^{th} experimental line at the 9 MV Tandem Accelerator at IFIN-HH

6.2.1 Experimental setup

The first control system presented in this section is the scattering chamber on the 4^{th} experimental line of the 9 MV Tandem Accelerator at IFIN-HH which can be seen in Fig. 6.1.

This came as an upgrade in which several new systems were developed and used i.e., the moving system, the gas control system and the acquisition system. The new system was commissioned during a HI-ERDA experiment in which a ^{63}Cu beam at 80 MeV was used with two thin targets. The moving system for the presented configuration worked in half-step mode, also having the possibility of offering 1/256 micro-stepping, thus improving an already good precision. The gas system performed within the expected range, taking from two minutes to four minutes to stabilize the pressure. The test using the two targets that were considered, Si+ZrO_2 and SiC, provided the expected results being able to see C, O_2, and Si and also the scattered Cu projectiles on the heavier Zr.

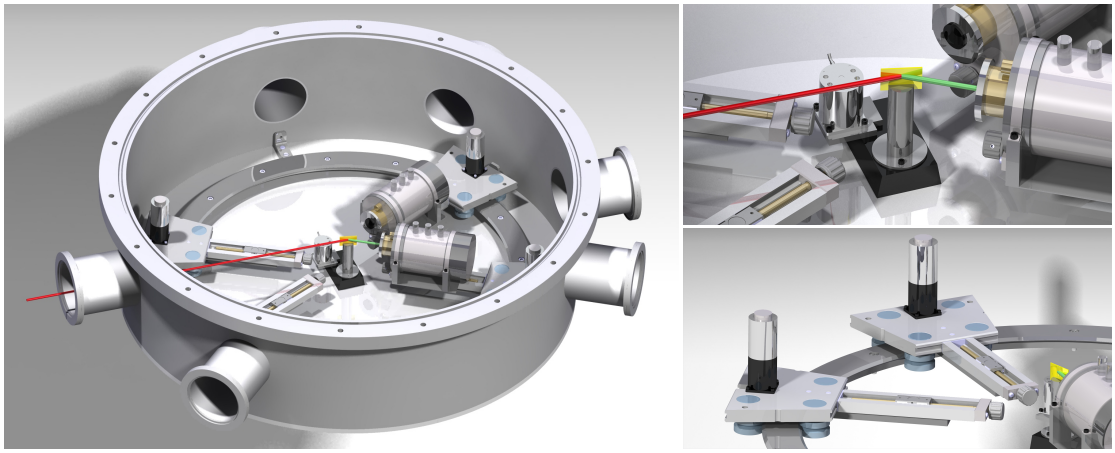

Fig. 6.1 (left) 3D render of scattering chamber with installed moving system and telescopes; (right top) Zoom-in on target holder (red – incident beam, green – scattered ions into the N-telescope, yellow - target); (right bottom) zoom-in on two guiding systems.

6.2.2 LabVIEW application

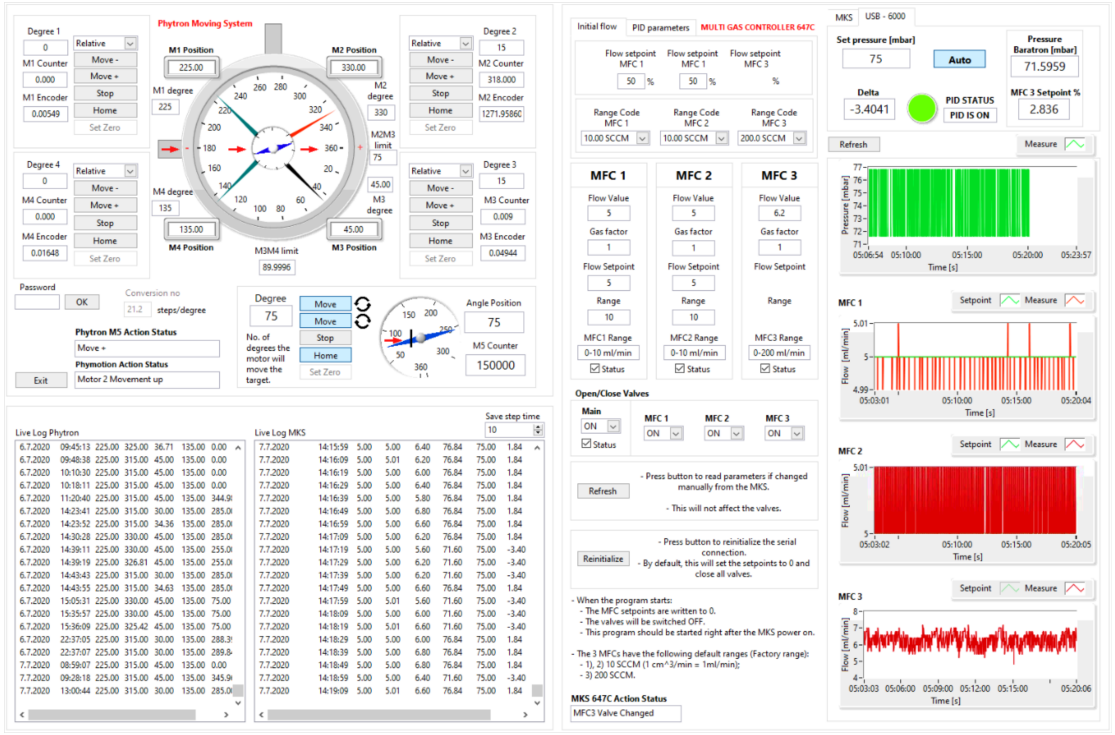

Fig. 6.2 LabVIEW interface for the control system. (left) the 4-arms and target movement control. (right) complete gas system control.

The user interface, as it can be seen in Fig. 6.2, was designed to fit a 19" monitor screen and have all the settings, measurement plots and data logging for both the gas system and moving system on the same interface. The moving system is represented by a four-needle gauge, each representing the four quadrants of the scattering chamber. Each motor has specific software implemented limits for the motors to not hit each other. These can be easily modified if one wants to change the detectors. Each arm is powered

by a stepper motor capable of relative and absolute movement. Although, the mechanical counter has proven its effectiveness, not giving any faulty readings, each motor also provides an encoder readout as a witness to the actual position. Each motor can be stopped at any moment, even if the arm is moving, can be homed and its "set zero" position can be adjusted only if the user inserts the password for that operation. The latter procedure i.e., "set zero" is done every time the alignment procedure is performed.

6.2.3 Measurements and system performance

This control system and performed measurements have been presented in detail in [21] which represent the original basis of the section.

- Nuclear Instruments and Methods in Physics Research Section B: Beam Interactions with Materials and Atoms, entitled: "Experimental set-up for high precision nuclear physics measurements at the IFIN-HH 9MV tandem accelerator", A.N.State, H.Petrascu, D.G.Ghita, Volume 499, 15 July 2021, Pages 53-60. https://doi.org/10.1016/j.nimb.2021.05.002

6.3 Control system based on Actor Framework and CS++ in LabVIEW - the slow control system of the FRS Ion Catcher at GSI

6.3.1 The FRS-IC experimental setup

The second part of Chapter 6 emphasizes the work that has been done to implement the FRS Ion Catcher Slow Control in the Actor Framework using the CS++ classes and utilities in LabVIEW. The FRS Ion Catcher (FRS-IC) [12] uses these fragments to perform experiments of exotic nuclei at low energies. It consists of a cryogenic stopping cell (CSC) to thermalize the exotic nuclei [22], a Radio Frequency Quadrupole (RFQ) beamline for mass selection and transport [23] and a Multiple Reflection Time of Flight Mass Spectrometer (MR-TOF-MS) including an RF trap system for ion sample preparation and an electrostatic analyzer for yield and mass measurements [24, 25]. Fig. 6.3 depicts the CSC and part of the RFQ beamline (DU1 — Diagnostics Unit 1) and shows the devices used to test the stability of the new system with its new functionality.

Throughout the system, high purity helium is used as buffer gas. Due to the high ionization potential of He, ions remain charged after thermalization in the CSC. They are transported with DC fields, created by an array of ring electrodes called the DC Cage, from the bulk of the CSC to a repelling RF structure (RF carpet). There, with combined DC and RF fields, ions are guided towards the extraction nozzle [26]. The length of the CSC stopping volume is defined by the length of the DC Cage which can

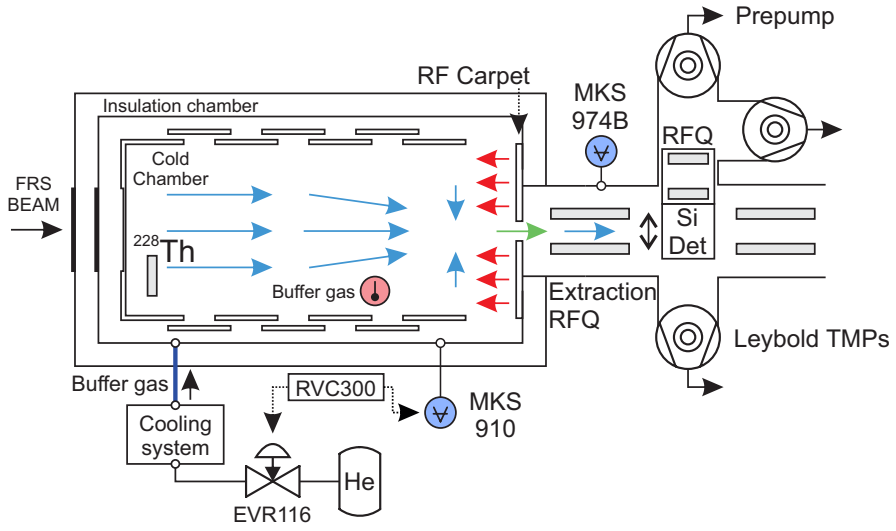

Fig. 6.3 Simplified schematic of the CSC and the first part of the RFQ beamline including a diagnostic unit (DU1) of the FRS-IC setup. For the commissioning of the slow control a silicon detector was used. Blue arrows represent DC fields, red arrows represent repulsive RF fields, green arrow represents the gas drag force. The Si detector can be exchanged with an RFQ for continuing the transport towards the remaining beamline and towards the MR-TOF-MS. The beam windows are displayed on the left.

be mechanically adapted to a specific experiment. Ideally, the maximal length is used, i.e., 1 m, but e.g., for short-lived nuclei higher extraction field strengths are favorable and thus shorter DC cage results in higher DC fields and thus faster extraction.

6.3.2 Control System Requirements

This section covers the requirements of the newly developed control system.

6.3.3 Slow control with the Actor Framework and CS++

Architecture

The utilized architecture with CS++ in LabVIEW is described in detail.

Implementation

The FRS-IC SCS was implemented using a distributed Client - Server architecture. This section describes in detail the implementation steps and developed control actors.

6.3.4 Graphical User Interfaces

The GUIs of the control system and their functionality are described. In Fig. 6.4 the MainGUI, i.e., the clients GUI, is depicted. On this interface, the operator, can see all values of intermediate interest, and control device parameters directly or launch GUIs for automated regulators.

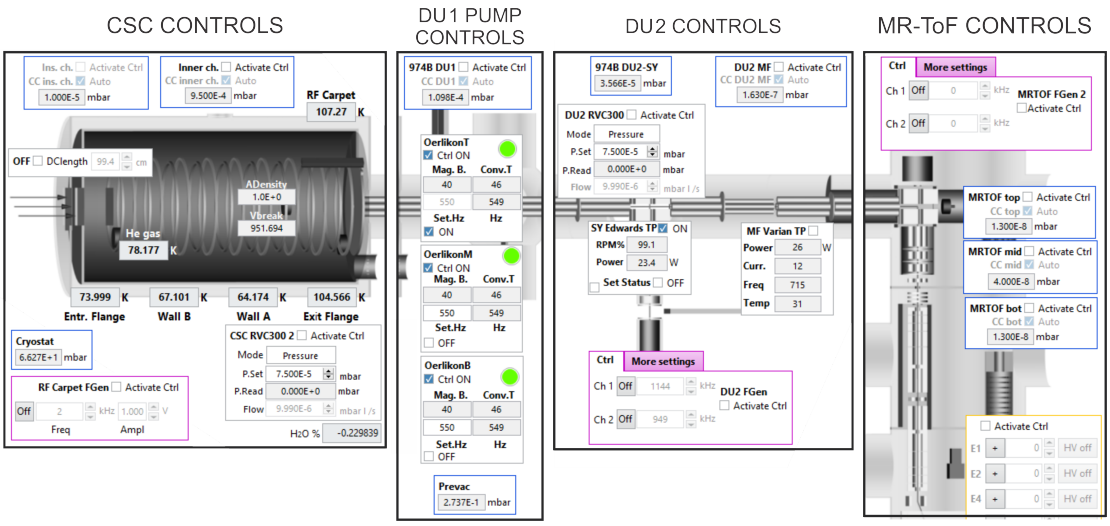

Fig. 6.4 Main parts of the graphical user interface for the MainGUI which is the main interface when starting the client application. The main parts of the system with their controls are delimited.

6.3.5 Measurements and system performance

An off-line test was performed using a ^{228}Th α-recoil ion source with the RF carpet set to 16 Vpp and 6.485 MHz. This contributed to the overall temperature of the system by the added heat. During this test, the cell was heated from approx. 85 K to 120 K. In order to express the extraction rates a silicon detector was used. In the extraction region an automated sled can change between an RFQ segment and a Si detector (Fig. 6.3). An areal density of 0.9 mg/cm^2 in the cell and an extraction pressure of 10^{-3} mbar were used (Fig. 6.5). Considering the total activity of the used ^{228}Th source of 7 kBq, the solid angles of the source holder and Si detector of 38% and 14%, with a survival efficiency of 50%, the estimated measured rate on the Si detector for ^{220}Rn is 0.121 kBq. The ions are transported 1.5 m from the source to the detector with the first decay product not seen as it has a very long half-life (^{224}Ra - 3.62 days). This measurement covers 6 hours of continuous operation in which the areal density in the cell and pressure in the extraction region were kept within $\pm$2% when compared to their setpoints. The RMS values are 0.8986 mg/cm^2 for areal density and 0.001 mbar for DU1 Pressure. This is within the expected variation that was foreseen for the setup.

The rate of ^{220}Rn (the 2^{nd} daughter isotope of ^{228}Th) is displayed in Fig. 6.5e). By minimizing the gas density fluctuations in the stopping cell and pressure fluctuations in the extraction region, with the SCS, a stable operation is achieved which leads to a constant extraction rate. Furthermore, the system can now be used for rare decay experiments that make use of the setup and are expected to last, in some cases, for several continuous months. The new SCS implementation with its control actors provides stable and controlled conditions both in terms of areal density in the cryogenic stopping cell and pressure in the extraction region. These lead to a stable extraction efficiency from

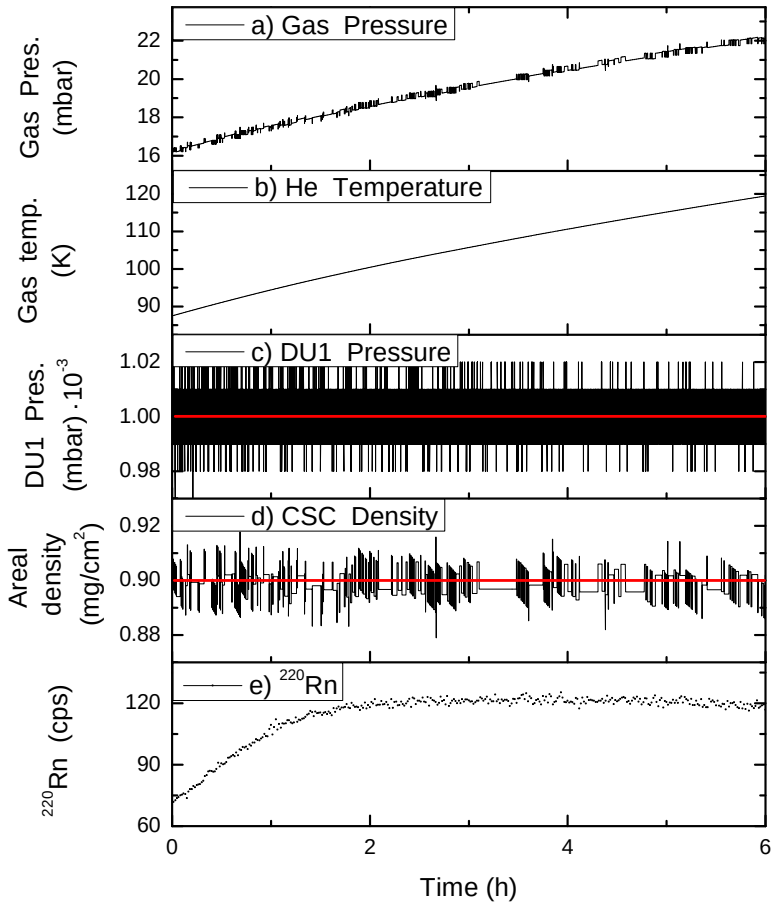

Fig. 6.5 a) He pressure in the gas cell. b) He temperature in the gas cell. c) Pressure in the extraction region. d) Areal density in the cell. e) ^{220}Rn rate in the Si detector over 6 hours. Red lines indicate the desired set value.

the CSC and a constant extraction rate over long periods of time whilst minimizing the needed human intervention.

Furthermore, long term stability tests both in pressure and density, when perturbations were created, proved the system is working within the expected parameters. The slow control system, with the Actor Framework and CS++ classes and utilities will be able to scale very efficiently through the years while more equipment will be added to it. In terms of memory usage and CPU load, the current SCS version occupies approx. 500 MB of RAM memory with less than 10% CPU load of an Intel Xeon W-2123 processor, having more than 1000 process variables. Thus, the system can readily reach a factor 2 to 3 more in terms of equipment and processes numbers. The new features provided by the SCS, such as pressure regulation, density regulation, breakdown voltage calculator, datalogger as well as the ease of building simple programs that use the network shared variables enhance the user experience and also expand the possibility of future experiments that require good stability. This work is based on the several research stages at GSI, Germany and also on the original work published in [27]:

- Nuclear Instruments and Methods in Physics Research Section A: Accelerators, Spectrometers, Detectors and Associated Equipment, entitled: "The slow control system of the FRS Ion Catcher", A.N.State, S.Beck, D.Amanbayev et al, Volume 1034, 1 July 2022, 166772. https://doi.org/10.1016/j.nima.2022.166772

6.4 Summary of Chapter 6

A short overview and summary of the chapter is provided in the thesis. This also emphasizes the original work of the author.

Chapter 7

Conclusions and perspectives for further developments

Exotic nuclei represent the key quest of our generation which might answer many questions that are still troublesome. Out of the many aspects, astrophysics is one that benefits greatly from the investigations of neutron-rich exotic nuclei by providing missing pieces to the nucleosythesis puzzle. In our pursuit of knowledge, new technologies and methods are constantly developed to access more and more shorter life-times. These impact greatly also our society, maybe not on short-term, but on long-term, they will lead to progress.

Two methods of production and separation are currently in use in various different forms: the in-flight and the isotope separation on-line (ISOL). An overview has been presented in Chapter 2 of the thesis. Various equipment with different approaches are used at different facilities with the common goal of searching and investigating unknown exotic neutron-rich nuclei. This search is done with great effort that lasts many years before an actual experimental setup is at a sufficient maturity level to provide RIBs of new and undiscovered nuclei. Such an experimental setup is the HADO-CSC. It provides an orthogonal extraction, that leads to a fast extraction time ($\approx$ 10 ms) and works at cryogenic temperatures for an increased density and purity of the gas. The fission products, formed after the interaction of the ELI-NP gamma beam with the thin actinide targets placed inside the gas cell, are trapped in the buffer gas and undergo a process of thermalization. The latter is very favorable, as the fission products remain in a plus charge state due to the high ionization potential of helium. As supersonic jets are meant to be used as a guiding mechanism with the HADO-CSC, several different studies to better understand the physics behind their formation were needed.

Chapter 3 emphasizes the work that was done whilst using Comsol Multiphysics with the CFD Module and more specifically the high mach number flow module. The latter is specifically designed for jets at high mach numbers and solves the compressible Navier-Stokes equations. Before performing simulations of cylindrical nozzles, which will be used for the HADO-CSC, Laval nozzles were simulated in order to test the

simulation program. A converging-diverging nozzle, which has the advantage of being described analytically by the area-mach number relation, was used. Considering an isentropic flow through the nozzle, the results obtained from the simulations are in good agreement to the analytical values with less than 2% differences at the sonic and outlet lines proving the simulation program performs as expected. Moreover, the original work also involved a MATLAB code that is based on the normal-shock equations and the bisection method. Two cases for the outlet pressure of the nozzle were considered: 3 mbar, which is the outlet pressure for an isentropic flow through the nozzle and 200 mbar, which is a drastic change in the outlet pressure. The position in the divergent section where a normal shock is formed was compared between the analytical result and the performed simulation. The results are in good agreement with an error in the normal shock position less than 2%.

Moreover, in order to perform a complete study of a geometry where the boundary conditions are placed at the inlet and outlet ports of the chamber and not the inlet and outlet ports of the nozzle, a smaller scaled geometry was designed. This has the same ratio between the stopping chamber and extraction chamber volumes of 1:4 and uses only two nozzles. By doing this, the required memory needed for the simulation is decreased. In order to further investigate the behavior the jets, the same Laval nozzle was used. The slight higher pressure at the nozzle outlet limited the Mach number value to 3.81 also indicating an under-expanded jet. A thousand ^{145}Ce ions were released uniformly from the nozzle inlet. These ions were selected because the ELI-NP IGISOL facility will be focused on the respective region. By using the drag force generated by the supersonic jets the ions follow the gas streamlines and cover a distance of 10 cm and reach the RF Carpet at an average velocity of 10.2 m/s. This velocity is of great importance as the current designs of RF Carpets only admit a velocity of $\approx$ 50 m/s in order to catch the ions. The mass flow rates through the system are of great importance as they dictate the gas system components used for the gas cell. Under the assumption of a closed system with possible leaks neglected, the mass flow rate can be considered as $n \cdot \dot{m}_{nozzle}$, where n - number of nozzles and $\dot{m}_{nozzle}$ is the mass flow rate through one nozzle. For the considered laval nozzle a mass flow rate of $\approx$ 0.22 g/min is needed for a 300 - 3 mbar pressure drop. All the original work that is emphasized in Chapter 3 has been published in [28].

Chapter 4 is focused on the conceptual design of the Helium Recovery Unit. This is a cost-effective gas system that maintains stable operation in terms of pressure in the two chambers of the HADO-CSC. At the same time is provides a recirculation system to decrease the operational cost of the gas that the cell uses. In terms of mechanics, it provides a modular design which can be assembled and later on craned down to its specific location. It weights $\approx$ 1.2 t, with all the components, found in the different modules of the HRU, distributed uniformly. The HRU is a closed system with a dust filter mounted near the main heat sources and a series of fans, connected to the control system.

These will maintain a constant temperature inside. By considering the full power load of $\approx$ 4.5 kW a flow of 48 m^3/h to maintain a 5°C difference was calculated. Two buffer vessels were considered to be placed between the compressor and the fluctuating pressure. By doing this, the compressor lifetime is greatly improved and also stability increases. This is achieved by minimizing the loading and unloading cycles of the compressor. A standard He 6.0 50-liter, 200 Bar, holds a quantity of He of $\approx$ 1.78 Kg. By considering all the masses and flow rates required to maintain the HADO-CSC conditions (Pressure vessel - 167 g, Vacuum vessel - 17 g, Stopping chamber - 161 g, Extraction Chamber - 0.27 g (2 mbar), 1.37 g (10 mbar), mass flow rate (St. Ch. - Extr. Ch) $\approx$ 4.12 g/min) with a 0.16% loss through the RFQ), the HRU is capable of reaching 37 days of continuous operation before changing the He bottle. Furthermore, the command system is based on a PXI chassis which has a modular design and programmed with LabVIEW. Each corresponding module serves a different task related to the HRU. More specifically, a relay module will be used to address the overall control of all the solenoid valves through the system, and for witnesses a DI/DO module is used. Different serial modules (RS232, RS485) address the requirement of serial control and monitor of all the related equipment in the HRU, like vacuum and pressure gauges, compressor controller, control valves etc. Moreover, the HRU will be programmed in LabVIEW using the CS++ framework developed at GSI which extends the NI implementation of the Actor Framework. All the original work, i.e., conceptualization of the system, mechanical design, working and logical gas diagrams are contained within the Internal Design Report entitled: "Helium Recovery Unit for the LEB CSC", A. State and T. Dickel.

Chapter 5 focuses on the design, construction and implementation of the STU (Supersonic Test Unit). Such a setup represents the original work of the author to further compare simulations with actual empirical data at room temperature (RT) conditions. This setup is capable of reproducing the HADO-CSC pressure drops at RT being used with several different methods of characterization: Schlieren imaging, gas jet fluorescence, Pitot tube measurements. It is formed by two chambers; one acrylic vacuum chamber with a 30 L volume and an ISO-K DN160 4-way cross that are fixed together on a custom adapter plate. The obtained leak rate was 10^{-4} mbar·l/s so possible leaks in the system could be neglected. To further improve the overall easiness of changing and replacing the nozzles, the latter were drilled in small DN16 blind flanges. Several different diameters were used. A gas system for the STU was designed and built. This is based on two pressure regulators: one forward pressure regulator that maintains the pressure in the 4-way cross to a user decided value and a backward pressure regulator for the acrylic chamber. These regulators are achieved by controlling the control valve inside the used mass flow controllers that are used as control valves. A special remark can be made about the used inlet MFC, which is of Coriolis effect, used to measure and control the mass flow rate. This type of MFC is of particular interest as it can provide a direct measurement of the mass flow rate through the system, whereas the other MFC is

of thermal effect with less precision in measurement. The built control system is based on LabVIEW and it is based on a queued state machine architecture. It provides all the controls and monitoring of all the equipment involved in the measurements, like gas system controls, the moving system control, brightness control for the Schlieren light source, absolute pressure sensors used for the Pitot tube, datalogging, system information like CPU, RAM, HDD space etc.

Several different measurements were envisaged to be used with the STU. The first method relied on the Schlieren imaging technique in which light rays when passing a density gradient, induced by the jet, are distorted. This change in trajectory can then be used to show the plus and minus signs of the density gradient by positioning a knife edge to cut half of the focal point, before the camera. The add-ons that can be put on the STU and fixed on the frames provide two 8" parabolic mirrors mounted in high precision gimbals with their angles calculated beforehand in the design stage. The mirrors have an effective focal length of 48" and an average reflectivity above 95% in the 450 - 650 nm interval. Together with the STU they form a two-mirror Schlieren setup or sometimes called a Z-Schlieren setup. The system has been thoroughly aligned, in order to minimize the possible aberrations that might appear. Astigmatism cannot be fully eliminated and two focal points or image points ar formed. Several light sources have been tested, such as different LEDs of different wavelength and brightness and a HeNe laser but it can be concluded that the method is not at all sensitive to low density gradients where pressure is small. Although used extensively as a standard method in characterizing gas targets in laser experiments the limits to which this method is applicable to free He jets is not stated clearly in literature. With the current setup, compressed air, with a density 3000 times larger than the one that was of interest can be clearly seen and characterized. The Gladstone-Dale formula that relates the refractive index to the medium density leads to a value of the refractive index of $\approx$1.0003215 at a density for helium of 0.00164 kg/m^3 which implies a very good sensitivity which cannot be accomplished with the current setup. A future study in which several different gases will be used will address the physical limits to which such an optical method is applicable and also it will be extended to other non-invasive optical methods.

A second measurement that was performed implied using a Pitot tube. The latter represents a flow measurement device with which one can measure the total and static pressures along the jet axis. By doing this, pressure profiles along the jet axis can be done and under certain assumptions velocity can be approximated using Bernoulli's equation. The latter, requires the assumption of an inviscid, incompressible flow and by knowing the difference between the two pressures and the flow density at the tip of the Pitot tube one can approximate velocity. In order to have repetitive and accurate measurements a moving system was constructed. This is based on two high-precision linear stages which were fitted with stepper motors. The motors are used in full-step mode being driven by small drivers placed on a small development board that is controlled via LabVIEW.

Two modes of operation are intended to be used with the current setup. An XY mode which can be used for mapping and an XZ mode which can be used for performing axial measurements. The space restrictions inside the chamber lead to a coverage of the pressure along the jet axis of only 6.2 cm. As such, a 0.5 mm nozzle was used. This nozzle diameter was selected as higher diameters lead to higher velocities. This statement is assumed based on the gas jet fluorescence measurements which provide more jet intensity in regions close to the Pitot tube position as one increases the nozzle diameter. Moreover, the 0.5 mm nozzle does not present an observed bow shock (curved normal shock) forming at the tip of the Pitot tube. This behavior would be an indicator that the jet has a high Mach number and the total pressure measured by the Pitot tube is not the one that is desired, and one would measure the pressure behind a normal shock which would indicate a smaller pressure value. A pressure difference $P_{tot} - P_{st}$ of 0.2 mbar which is found at 6.2 cm would translate to a velocity of $\approx$ 150 m/s at a gas density of 0.00215 kg/m^3. The latter density is considered from the NIST database of thermodynamic properties of Helium at 12.2 mbar and 18°C. The temperature has been measured using a PT100 placed inside the chamber right at the tip of the Pitot tube. The used absolute pressure sensors is prone to very large errors due to the accuracy of $\pm$2.5 mbar. Moreover, a variation of $\pm$0.25 mbar leads to a variation in velocity of $\pm$75 m/s. The static pressure does not have a strong change, leading to just 1 mbar variation from the nozzle outlet to the maximum point at which the setup can be used. As such, only the total pressure is the one that is important to be known. Based on the measured pressure along the 6.2 cm and extrapolating, after $\approx$ 1 cm the total pressure would match the static pressure. This indicates a small pressure difference which in turn leads to a low velocity, as seen in the simulation results.

Gas jet fluorescence has been used with the STU. Although the results obtained with this method are more on the qualitative side, its results can be used to better quantify the behavior of the pressure on the jets. A single needle electrode is placed right before the nozzle output on which high voltage is applied from an external power supply. After 450 V the emerging jet exhibits a visible glow corresponding to the excited states of helium. By using a wide range spectrometer connected to a fiber optics placed in front of the jet one can see the possible impurities that appear in the chamber. Nitrogen lines, that appear in the optical emission spectrum, are filtered with the use of a colored filter, that will cut all wavelengths smaller than 600 nm. By doing so, only the wavelengths emitted by helium are used in the post-processing of the jet pictures. Nozzles with different diameters: 0.5, 0.7, 0.9 mm were used. Based on the region of interest different exposure times are used. If one assumes the jet physical characteristics, as shape and size, are proportional to gas velocity induced by the pressure drop, one can express some rules of thumb in the behavior of the jet. When increasing the backing pressure, each 25 mbar leads to an increase in intensity of 100%. This behavior is met for all nozzles. When comparing the maximum intensities between different diameters one can

see a factor of ten between 0.5 mm and 0.7 mm nozzles with a factor three difference between the 0.7 mm and 0.9 mm. Moreover, a 0.5 mm nozzle will provide information from the fluorescence technique, in the considered region (10 cm), only starting with a pressure drop of 250 - 10 mbar. The 0.9 mm saturates at the same maximum intensity due to reaching the ends of the picture. It can be concluded that whilst maintaining the same background pressure, modifying the backing pressure leads to a longer seen jet, corresponding to a higher velocity. The gas jet fluorescence gives information also on the behavior of the jet when modifying the background pressure. Whilst maintaining a constant pressure of 300 mbar the background pressure was modified with one mbar at a time. It can be concluded that increasing the background pressure, the FWHM is also increasing. The height of the intensity distribution increases with $\approx 10\%$ for each added mbar whilst the FWHM increases by $\approx 5\%$. These studies can be concluded with the following remarks. The backing pressure increases the length of the jet whilst maintaining a similar FWHM, thus a higher jet velocity will be met at 10 cm. The background pressure results in two jet effects: a higher background pressure results in a smaller FWHM and a lower velocity of the jet.

Furthermore, the jets in the HADO-CSC will all be highly underexpanded leading to a shock cell pattern with a normal shock present in the shock cells. Based on the empirical formula that predicts the location of this normal shock, its position is calculated and compared to both the simulation and location as observed from the jet fluorescence. The results are in good agreement with the expected location. Moreover, from the position of the normal shock one can also calculate the background pressure which falls between 8 - 12 mbar. This uncertainty is given by the uncertainty in the selection of the normal shock in the taken pictures. Based on all the studies a 0.4 - 0.5 mm nozzle will lead to the expected velocities at 10 cm where the RF Carpet is placed. A larger nozzle diameter will need either a lower pressure in the extraction region or a larger height for the extraction chamber.

The STU will be used in the near future with actual PCBs (Printed Circuit Boards) that represent the RF Carpets, as the nozzles will be the ones resulted in the whole deposition and milling processes. As the RF carpet is multilayered, a direct comparison will be made with the ones presented in the current work, milled in aluminum, and the ones in the resulting RF Carpets. Furthermore, the direct pressure measurement will be repeated with the Pitot probe placed in the middle of an RF Carpet, reproducing the application even more. Another planned experiment with the STU is represented by the use of a particle source, more explicitly a ^{223}Th in tandem with a Si detector. The latter will be placed on the XY moving system with an Al foil in front of it, with the source placed behind the nozzle. This will provide a direct measurement of the efficiency of the transportation to optimize the jets even further.

Chapter 6 has treated in detail two original control systems, used in nuclear physics experiments, that rely on different design patterns developed in LabVIEW. The first

one represents the control system of the scattering chamber at the 4^{th} experimental line of the 9 MV Tandem Accelerator found in IFIN-HH. It is based on a queued message handler which provides a way of running parallel code, sending data between the various loops and communicate via messages. This design represents a combination of the producer-consumer and event handler architectures where the first producer loop is called the Event Handler Loop (EHL) and reacts to events triggered by the user through interactions with the front panel controls by sending messages to the consumer loop, caller the Message Handler Loop (MHL) which executed on the incoming messages. This control system that provides a way of controlling and monitoring various equipment, like pressure gauges, gas system, vacuum system, moving system was tested and successfully commissioned during a HI-ERDA experiment in which a ^{63}Cu beam at 80 MeV was used with two thin targets: SiC and Si+ZrO_2. This experiment proved the reliability and reproducibility and precision of the newly developed system. This control system was presented in detail in [21], which represents the original contribution of the author to this chapter.

A second control system was treated in detail i.e., the slow control of the FRS Ion Catcher. The latter represents a setup that slows down the exotic nuclei produced with the Fragment Separator (FRS) at GSI and is able to perform precision measurements. The main focus of the new control system based on CS++ and Actor Framework in LabVIEW has been to improve the overall operational stability of the CSC while providing other features: like automated data-logging, interactive GUIs, seamless operation over a wide range of computers on the local network. It also offers the possibility of creating automated processes, e.g., pressure control feedback loops and alarm monitoring whenever a fault occurs. The system is meant to read, process and archive a few thousand network-shared process variables. This is achieved by using the already-built network infrastructure, in which all devices are connected to serial to network servers. Furthermore, such an improvement was necessary due to the need of stable operation with limited human intervention, over long periods of time, as new experimental programs are developed with an intended run time of several months.

Two control actors have been developed in order to keep stable the areal density inside the cell and the pressure in the extraction region. The slow control system has been commissioned in an off-line experiment in which a ^{228}Th α recoil ion source was used. The RF Carpet was operated at 16 Vpp and 6.485 MHz. In order to test the stability of the slow control system, the temperature of the gas was heated from $\approx$85 K to 120 K. In order to express the extraction rates a Si detector was used, placed at 1.5 m from the source position, in the first diagnostics unit. A measurement of ^{220}Rn over six hours in the Si detector in which the areal density in the cell and the pressure in the extraction region were kept within $\pm$2% when compared to their setpoint, provided a stable and constant extraction rate. The system can be used for rare decay experiments that make

use of the setup and are expected to last, in some cases, for several continuous months. This part is based on the original work published in [27]:

List of publications

- **Characterization of X3 Silicon Detectors for the ELISSA Array at ELI-NP**, S. Chesnevskaya, D.L. Balabanski, D. Choudhury, M. La Cognata, P. Constantin, D.M. Filipescu, D.G. Ghita, G.L. Guardo, D. Lattuada, C. Matei, A. Rotaru, C. Spitaleri, **A. State**, Y. Xu. EPJ Web Conf., (**2017**).

- **Performance studies of X3 silicon detectors for the future ELISSA array at ELI-NP**, S. Chesnevskaya, D.L. Balabanski, D. Choudhury, P. Constantin, D.M. Filipescu, D.G. Ghita, G.L. Guardo, D. Lattuada, C. Matei, A. Rotaru, **A. State**, J. Instrum. 13 (**2018**).

- **Ion beam optic simulations at the 1MV Tandetron from IFIN-HH Bucharest**, D. Pacesila, D. Ghita, T. Sava, M. Straticiuc, V. Mosu, A. Rotaru, **A. State**, O. Gaza, G. Cata-Danil. Romanian Reports in Physics, 71, 204 (**2019**).

- **Simulation of circular radio-frequency carpets for ion extraction from cryogenic stopping cells**, A. Rotaru, G. Căta-Danil, P. Constantin, D.L. Balabanski, T. Sava, **A. State**, A. Spătaru, D. Nichita. UPB Sci. Bull. Ser. A Appl. Math. Phys. 81 (**2019**).

- **Status of ELI-NP and opportunities for hyperfine research**, D.L. Balabanski, P. Constantin, A. Rotaru, **A. State**, Hyperfine Interactions, 240 (**2019**).

- **The cryogenic stopping cell of the IGISOL facility at ELI-NP**, P. Constantin, A. Rotaru, **A. State**, D. Nichita, A. Spataru, D.L. Balabanski, T. Sava, M. Merisanu, T. Roman, C. Scheidenberger, T. Dickel, W.R. Plass. Nuovo Cim. Della Soc. Ital. Di Fis. C. 42 (**2019**).

- **The ELI-NP IGISOL radioactive ion beam facility**, P. Constantin, D.L. Balabanski, **A. State**, A. Rotaru, D. Nichita, A. Spataru, T. Dickel, W.R. Plaß, C. Scheidenberger, Nucl. Instruments Methods Phys. Res. Sect. B Beam Interact. with Mater. Atoms. 461 (**2019**).

- **Applications at the 3 MV TandetronTM from IFIN-HH**, I. Burducea, A. Mitu, A. Rotaru, A. Rugină, **A. State**, A. Vasiliu, B. Savu, D. V. Moşu, D. Iancu, D. A. Mirea, D. Păceşilă, P. Mereuţă, R. F. Andrei, T. B. Sava, and M. Straticiuc, AIP Conference Proceedings 2076, 050001 **(2019)**.

- **Ion extraction from gas cells with supersonic jets formed in laval nozzles**, **A. State**, M. Merisanu, D.L. Balabanski, P. Constantin, T. Sava, A. Rotaru, T. Roman, D. Nichita, A. Spătaru, W.R. Plaß. UPB Sci. Bull. Ser. A Appl. Math. Phys. 82 (**2020**).

- **Multi-nucleon transfer reactions in 238U + 64Ni using grazing model**, A. Spătaru, T. Dickel, W.R. Plaß, J.S. Winfield, P. Constantin, D.L. Balabanski, D. Nichita, A. Rotaru, **A. State**, UPB Sci. Bull. Ser. A Appl. Math. Phys. 82 (**2020**).

- **Optimization of photo-fission fragment production in the Elisol setup at ELI-NP**, D. Nichita, P. Constantin, D.L. Balabanski, B. Mei, A. Rotaru, T. Sava, A. Spătaru, **A. State**, T. Dickel, B. Kindler, B. Lommel. UPB Sci. Bull. Ser. A Appl. Math. Phys. 82 (**2020**).

- **Preliminary results on the measurement of plutonium isotopic ratios at the 1mv Ams facility in IFIN-HH**, D.G. Pacesila, A.R. Petre, E. Chamizo Calvo, A.I. Rotaru, **A. N. State**, V.D. Mosu, M. Virgolici, G. Căta-Danil. UPB Sci. Bull. Ser. A Appl. Math. Phys. 82 (**2020**).

- **Production of exotic nuclei via MNT reactions using gas cells**, A. Spătaru, D.L. Balabanski, O. Beliuskina, P. Constantin, T. Dickel, C. Hornung, A. Kankainen, A.V. Karpov, D. Nichita, W. Plass, S. Purushothaman, A. Rotaru, V.V. Saiko, **A. Stat**e, J.S. Winfield, A. Zadvornaya. Acta Phys. Pol. B. 51 (**2020**).

- **The IGISOL Facility at ELI-NP**, Dimiter L. BALABANSKI, Adrian ROTARU, **Alexandru STATE**, Mihai MERISANU, Le Tuan ANH, Tiberiu SAVA, Dan GHITA, Christoph SCHEIDENBERGER, Timo DICKEL, Wolfgang R. PLASS, Proceedings of 10th International Conference on Nuclear Physics at Storage Rings (STORI'17)

- **Mass measurements of As, Se and Br nuclei and their implication on the proton-neutron interaction strength towards the N=Z line**, I. Mardor, S. Ayet San Andrés, T. Dickel, D. Amanbayev, S. Beck, J. Bergmann, H. Geissel, L. Gröf, E. Haettner, C. Hornung, N. Kalantar-Nayestanaki, G. Kripko-Koncz, I. Miskun, A. Mollaebrahimi, W. R. Plaß, C. Scheidenberger, H. Weick, Soumya Bagchi, D. L. Balabanski, A. A. Bezbakh, Z. Brencic, O. Charviakova, V. Chudoba, Paul Constantin, M. Dehghan, A. S. Fomichev, L. V. Grigorenko, O. Hall, M. N. Harakeh, J.-P. Hucka, A. Kankainen, O. Kiselev, R. Knöbel, D. A. Kostyleva, S. A. Krupko, N. Kurkova, N. Kuzminchuk, I. Mukha, I. A. Muzalevskii, D. Nichita, C. Nociforo, Z. Patyk, M. Pfützner, S. Pietri, S. Purushothaman, M. P. Reiter, H. Roesch, F. Schirru, P. G. Sharov, A. Spătaru, G. Stanic, **A. State**, Y. K. Tanaka, M. Vencelj, M. I. Yavor and J. Zhao, Phys. Rev. C 103 (**2021**)

- **Experimental set-up for high precision nuclear physics measurements at the IFIN-HH 9MV tandem accelerator**, **A. State**, M. Petrașcu and D. Ghiță, Nucl. Instruments Methods Phys. Res. Sect. B Beam Interact. with Mater. Atoms. 499 (**2021**).

- **INCREASE: An in-cell reaction system for multi-nucleon transfer and spontaneous fission at the FRS ion catcher**, Adrian Rotaru, Daler Amanbayev, Dimiter L.Balabanski, David Benyamin, Paul Constantin, Timo Dickel, Lizzy Gröf, Israel Mardor, Ivan Miskun, Dragos Nichita, Wolfgang R. Plaß, Christoph Scheidenberger, Anamaria Spătaru, **Alexandru State**, Nucl. Instruments Methods Phys. Res. Sect. B Beam Interact. with Mater. Atoms. 512 (**2022**).

- **ELIGANT-GN — ELI Gamma Above Neutron Threshold: The Gamma-Neutron setup**, P.-A. Söderström, E. Açıksöz, D.L. Balabanski, F. Camera, L. Capponi, Gh. Ciocan, M. Cuciuc, M. Filipescu, I. Gheorghe, T. Glodariu, J. Kaur, M. Krzysiek, C. Matei, T. Roman, A. Rotaru, A.B. Şerban, **A.State**, H. Utsunomiya, V. Vasilca, Nucl. Instrum. Methods Phys. Res. Sect. A-Accel. Spectrom. Dect. Assoc. Equip., 1027 (**2022**).

- **The slow control of the FRS Ion Catcher**, **A. N. State**, S. Beck, D.Amanbayev, D. L. Balabanski, H.Brand, P.Constantin, T. Dickel, C. Hornung, D. Nichita, W. R. Plaß, H. Roesch, A. Rotaru, C. Scheidenberger, J. Siebring, A. Spataru, N. Tortorelli, J. Zhao, Nucl. Instrum. Methods Phys. Res. Sect. A-Accel. Spectrom. Dect. Assoc. Equip., 1034 (**2022**).

- **Spiral RF carpet for ion mass spectrometry with radioactive isotope beams**, A. Rotaru, P. Constantin, D.L.Balabanski, D. Nichita, A. Spătaru, **A.N. State**, Int. J. Mass Spectrom., 478 (**2022**).

List of significant international schools and conferences:

- Young Researcher & Young Engineer Days - ELI-NP 2021 Edition: "Characterization of gas jets using the Supersonic Test Unit at ELI-NP", 1st Prize, **Oral presentation**.

- Carpathian Summer School of Physics 2021 (18.08.2021 - 27.08.2021) - "RIB formation with supersonic jets at ELI-NP" - **Oral presentation**:

- EURORIB 2018 (27/05/2018 – 01/06/2018) - "Gas flow simulations in the cryogenic stopping cell for the IGISOL facility at ELI-NP" - **Poster presentation**:

- Developments and solutions for the cryogenic stopping cells at LEB/FAIR and ELI-NP 26.04.2018, CFD simulations and gas system design for the HADO-CSC - **Oral presentation**.

- ChETEC Training School in Nuclear Astrophysics Using Direct Methods (10.04.2018 - 21.04.2018).

- 15th Russbach School on Nuclear Astrophysics (18.03.2018 - 23.03.2018).

Research stages:

- 01.10.2018 – 30.11.2018 – GSI Helmholtz Centre for Heavy Ion Research GmbH, FRS Ion Catcher.
- 20.01.2020 – 31.01.2020 – GSI Helmholtz Centre for Heavy Ion Research GmbH, FRS Ion Catcher.
- 01.11.2020 – 21.12.2020 – GSI Helmholtz Centre for Heavy Ion Research GmbH, FRS Ion Catcher.

References

[1] T. Dickel et al. Conceptional design of a novel next-generation cryogenic stopping cell for the Low-Energy Branch of the Super-FRS. Nucl Instrum Methods Phys Res B 376 (2016) 216-220.

[2] D. L. Balabanski, F. Ibrahim, and et al. Photofission experiments at ELI-NP. Rom. Rep. Phys., 68, S621-S698, (2016).

[3] Hendrik Schatz and Klaus Balum. Nuclear masses and the origin of the elements. *Europhysics News*, 37(5):16–21, 2006.

[4] Y Blumenfeld, T Nilsson, and P Van Duppen. Facilities and methods for radioactive ion beam production. *Physica Scripta*, 2013(T152), 2013.

[5] M. Lindroos. Review of ISOL-type radioactive beam facilities. EPAC 2004, Lucerne, Switzerland.

[6] Symons T. J. M. et al. Observation of New Neutron-Rich Isotopes by Fragmentation of 205-MeV/Nucleon 40Ar Ions. Phys. Rev. Lett. 42, 40.

[7] John C. Cornell. Radioactive ion beam facilities in Europe: Current status and future development. GANIL, BP 55027, Caen 14076 cedex 5, France.

[8] Savard G. and Levand A.F. et al. The CARIBU gas catcher. Nucl Instrum Methods Phys Res B 376 (2016) 246-250.

[9] Gottberg A. Target materials for exotic ISOL beams. Nucl Instrum Methods Phys Res B 376 (2016) 8-15.

[10] Borge M.J.G. Highlights of the ISOLDE facility and the HIE-ISOLDE project. Nucl Instrum Methods Phys Res B 376 (2013) 408-412.

[11] Essabaa S. and Barre-Boscher N. et al. The radioactive beam facility ALTO. Nucl Instrum Methods Phys Res B 317 (2013) 212-222.

[12] W.R. Plaß, T. Dickel, and S. Purushothaman et al. The frs ion catcher – a facility for high-precision experiments with stopped projectile and fission fragments. Nucl Instrum Methods Phys Res B 317 (2013) 457–462.

[13] Constantin P. Design of the gas cell for the IGISOL facility at ELI-NP. Nucl Instrum Methods Phys Res B 397 (2017) 1-10.

[14] Purushothaman S. and et al. First experimental results of a cryogenic stopping cell with short-lived, heavy uranium fragments produced at 1000 MeV/u. Eur. Phys. Lett. 104 (2013) 42001.

[15] Aysto J. and et al. Development and applications of the IGISOL technique. Nucl Instrum Methods Phys Res A 693 (2001) 477-494.

[16] Nichita. D et al. Radioactive ion beam production at the Gamma Factory. Annalen der Physik (2021).

[17] Wada M. et al. Slow RI-beams from projectile fragment separators. Nucl Instrum Methods Phys Res B 204 (2003) 570-581.

[18] Ranjan M. New stopping cell capabilities: RF carpet performance at high gas density and cryogenic operation. EPL 96 (2011) 52001.

[19] COMSOL Multiphysics Reference Manual, version 5.1.

[20] J. D. Anderson. Modern Compressible Flow: With Historical Perspective, vol. 3, McGraw-Hill Professional, New York, 2002.

[21] A. N. State, H. Petrascu, and D. G. Ghita. Experimental set-up for high precision nuclear physics measurements at the IFIN-HH 9 MV Tandem Accelerator. Nucl. Inst. Meth. B, 499, 53-60 (2021).

[22] S. Purushothaman, M. P. Reiter, and E. Haettner et al. First experimental results of a cryogenic stopping cell with short-lived, heavy uranium fragments produced at 1000 MeV/u. EPL 104 (42001) (2013).

[23] Emma Haettner, Wolfgang R. Plaß, and Ulrich Czok et al. A versatile triple radiofrequency quadrupole system for cooling, mass separation and bunching of exotic nuclei. Nucl Instrum Methods Phys Rev B 880 (2018) 138–151.

[24] T. Dickel, W.R. Plaß, and A. Becker et al. A high-performance multiple-reflection time-of-flight mass spectrometer and isobar separator for the research with exotic nuclei. Nucl Instrum Methods Phys Res B 777 (2015) 172–188.

[25] Wolfgang R. Plaß, Timo Dickel, and Ulrich Czok et al. Isobar separation by time-of-flight mass spectrometry for low-energy radioactive ion beam facilities. Nucl Instrum Methods Phys Res B 226 (2008) 4560–4564.

[26] M. Ranjan, S. Purushothaman, and T. Dickel et al. New stopping cell capabilities: RF carpet performance at high gas density and cryogenic operation. EPL 96 (52001) (2011).

[27] A. N. State, S. Beck, and D. Amanbayev et al. The slow control system of the FRS Ion Catcher. Nucl. Inst. Meth. A, 1034, (2022).

[28] A. State, M. Merisanu, and D.L. Balabanski et al. Ion extraction from gas cells with supersonic jets formed in laval nozzles. UPB Sci. Bull. Ser. A Appl. Math. Phys. 82 (2020).